2021-01-05

Palaeozoic stromatoporoids and chaetetids analysed using electron backscatter diffraction (EBSD); implications for original mineralogy and microstructure

Balthasar, U

10.1007/s10347-020-00618-5
Facies
Springer Science and Business Media LLC

accepted on the 26th of November 2020

Palaeozoic stromatoporoids and chaetetids analysed using Electron Backscatter Diffraction (EBSD); implications for original mineralogy and microstructure

Uwe Balthasar[1], Stephen Kershaw[2*], Anne-Christine Da Silva[3], Barbara Seuss[4], Maggie Cusack[5], Kilian Eichenseer[1], Peter Chung[6]
1: School of Geographical, Earth and Environmental Sciences, Plymouth University, PL4 8AA, Plymouth; United Kingdom
2: Department of Life Sciences, Brunel University, Kingston Lane, Uxbridge, UB8 3PH, United Kingdom
3: Sedimentary Petrology, Geological Departement, Liège University, Liège, 4000, Belgium
4: GeoZentrum Nordbayern (GZN), Paläoumwelt, Friedrich-Alexander University Erlangen-Nürnberg, Loewenichstraße 28, 91054 Erlangen, Germany
5: Division of Biological & Environmental Sciences, Faculty of Natural Sciences, University of Stirling, Stirling, FK9 4LA, UK
6: School of Geographical & Earth Science, University of Glasgow, Glasgow, G12 8QQ, UK
*Corresponding author; Stephen.kershaw@brunel.ac.uk

Abstract

Palaeozoic hypercalcified sponges were ubiquitous Ordovician – Devonian reef builders but, despite their rich fossil record, their original skeletal mineralogy and microstructure remain poorly understood. This study provides the first application of electron backscatter diffraction (EBSD) to analyse skeletal structure of Silurian and Devonian stromatoporoids. The two Silurian and two Devonian stromatoporoid taxa selected are typical of stromatoporoids in showing poor preservation. A reference sample of an exceptionally well-preserved hypercalcified chaetetid sponge from the Carboniferous Buckhorn Asphalt Quarry (a fossil lagerstätte renowned for its preservation of skeletal microstructures) contains evidence that its skeleton comprised distinct bundles of single-crystal fibres, similar to modern hypercalcifying sponges. Similar bundles of crystal fibres are proposed here as the original microstructure of stromatoporoids, and acted as precursors to the coarse fibrous calcitic overprinting recrystallisation that is orientated normal to the growth layers, seen in all stromatoporoids viewed in cross-polarised light. The studied stromatoporoids show pronounced microporosity and micro-dolomite inclusions which are circumstantial evidence of an original composition of high-Mg calcite (HMC). We propose that the evidence of fibrous structures might be linked to inclusions of hydrated amorphous calcium carbonate (ACC·H_2O) in the skeleton at the time of early diagenesis, as occurs in modern calcified sponges. The possible HMC skeletal composition of Palaeozoic stromatoporoids supports earlier views that the mineral composition of hypercalcifying reef builders is linked to Phanerozoic oscillations in the ratio of Mg:Ca, expressed as aragonite-calcite seas; stromatoporoids thrived in times of calcite-seas.
(239 words)

Key words: stromatoporoid, chaetetid, sponges, micro-dolomite, high-magnesium calcite, aragonite-calcite seas

Introduction and aims

Sponges are intriguing for their ability to biomineralize a diverse range of minerals including aragonite, calcite, amorphous silica, and SiO_2-$CaCO_3$ composite materials (Ehrlich et al. 2010, 2011; Gilis et al. 2011, 2013; Smith et al. 2013). Siliceous spicules are the most common mineralised structure in sponges and only about 8% of the ca. 8000 species of extant sponges secrete calcareous structures (Uriz, 2006); these calcifying sponges are generally restricted to cryptic reef environments (Gilis et al. 2013 and references therein). Calcareous mineralisation takes two forms: 1) calcitic spicules, normally considered to be the part of the primary sponge structure; and 2) massive calcitic or aragonitic basal skeletons that constitute a secondary structure in hypercalcifying sponges. Although calcareous spicules are a synapomorphy (present in ancestral forms and inherited by later forms, applicable in this case to modern forms) of the class Calcarea (Manuel et al. 2004; Voigt et al. 2012), calcified basal skeletons are scattered among both calcareans and demosponges without any obvious phylogenetic significance (e.g. Voigt et al. 2012; Morrow & Cárdenas, 2015). Fewer than 20 genera of extant sponges are hypercalcifying (Smith et al. 2013), and none of them contribute significantly to modern-day reefs.

The present-day paucity of hypercalcified sponges and their minor role in reef systems is strongly contrasted by geological times when hypercalcified sponges were major reef builders (stromatoporoids during the Ordovician – Devonian) or reef components (chaetetids from the Devonian – Cretaceous and stromatoporoids during the Jurassic-Cretaceous) (Wood 1987; West 2012). However, despite their abundance in the fossil record, hypercalcified sponge calcification processes and original mineralogy are poorly understood because of pervasive recrystallisation that particularly affected stromatoporoids. Resolving this issue has application in two linked areas: 1) information on skeletal mineralogy will aid understanding of their biology of calcification; and thus, 2) the role of hypercalcified sponges in the debate regarding aragonite-calcite seas (Stanley & Hardie 1998). Therefore, the aim of this study is to advance understanding of skeletal structure and mineralogy of fossil hypercalcified sponges, using electron backscatter diffraction (EBSD), which, to our knowledge, has not been previously applied to these fossils. EBSD facilitates detailed analysis of crystal structure and orientation, not available by other means. The principal focus here is on Palaeozoic stromatoporoids because of their high-volume abundance in shallow-marine systems, and their long geological range (Middle Ordovician to Early Carboniferous, see Kershaw & Sendino 2020). However, available to the study is a well-preserved hypercalcified sponge chaetetid specimen from a Carboniferous Lagerstätte, that provides an important reference sample with which to compare middle Silurian and early Upper Devonian stromatoporoids, that is, time-periods when stromatoporoids left a rich fossil record. Because of the time-intensive process of EBSD study, we examine a limited number of specimens as a preliminary study to assess the viability of application of EBSD to this research area. We make inferences that may thus form the basis for more extensive study in future research.

Literature background and relevance of original mineralogy of stromatoporoids

Stanley and Hardie (1998) set out a case that, throughout the Phanerozoic Eon, the fluctuation in the Mg:Ca ratio of seawater and its influence on the primary $CaCO_3$

mineralogy had an important effect on the waxing and waning of the ecological importance of hypercalcified sponges. Those authors hypothesised that at times when Mg:Ca ratios were greater than two, aragonite precipitation was favoured ('aragonite seas'), whereas Mg:Ca ratios less than two favoured precipitation of calcite ('calcite seas') (see also Hardie 1996; Eichenseer et al. 2019). Stanley & Hardie (1998) argued that hypercalcified reef-building organisms are particularly susceptible to changes in aragonite-calcite sea conditions and that the type of skeletal mineralogy of dominant reef-builders coincides with either aragonite or calcite seas accordingly. With respect to sponges, they argued that the ecological dominance of Palaeozoic stromatoporoids is driven by the extensive calcite sea conditions that existed from the mid-Cambrian to the Early Carboniferous.

The interpretation of aragonite-calcite seas proposed by Stanley & Hardie (1998) relies on two key assumptions: (1) that among the multiple drivers of aragonite-calcite sea conditions, the Mg:Ca ratio is the main factor influencing the skeletal mineralogy of reef builders, and (2) that the original skeletal composition of fossil reef builders can be reliably determined. The first point has been challenged from the recognition by more recent work (Morse et al. 1997; Balthasar et al. 2011; Balthasar & Cusack 2015) which interprets $CaCO_3$ polymorph formation to have been driven by a combination of Mg:Ca ratio and temperature with the effect that, contrary to Stanley & Hardie (1998), warm shallow-water seas probably experienced aragonite-facilitating conditions throughout the Phanerozoic. However, recent work that combined Phanerozoic records of temperature and Mg:Ca ratios showed that even when corrected for the effect of temperature, aragonite-calcite sea conditions significantly relate to the ecological success of marine calcifiers throughout the Palaeozoic (Eichenseer et al. 2019).

The second assumption, the unambiguous identification of the original skeletal composition, is unresolved for Palaeozoic stromatoporoids, the dominant group of hypercalcified sponges in the fossil record. Although individual stromatoporoids often formed massive decimetre-sized skeletons that typically show a characteristic internal architecture of vertical and transverse skeletal elements (Fig. 1), the reconstruction of primary skeletal composition is hampered by consistent recrystallization in the form of large irregular calcite crystals cutting across this internal architecture (Kershaw 2013). This type of preservation appears to be unique to stromatoporoids and presents a challenge to determine the primary skeletal composition. Although all Palaeozoic stromatoporoids are now calcite, their recrystallized nature has been interpreted by some authors as reflecting an original aragonitic skeleton (e.g. Semeniuk 1971; Stearn & Mah 1987; Mallamo & Stearn 1991), supported by increased levels of strontium in a single spicule-bearing specimen (Da Silva et al. 2014). Other authors, however, have identified abundant micro-dolomite, which points to an original high-magnesium calcite (HMC) composition (e.g. Rush & Chafetz 1991; Yoo & Lee 1993). When considering that extant hypercalcified sponges construct their basal skeletons of aragonite, low-Mg calcite (LMC), or high-Mg calcite (HMC) (Smith et al. 2013), it is reasonable to expect that all these skeletal compositions were feasible for sponges at any time in the past. However, because stromatoporoids exhibit the same preservational style, described by Kershaw (2013), this is circumstantial evidence that they possessed the same original skeletal composition.

Reconstructing the original mineral composition of calcareous grains in limestone is challenging because, over geological time scales, aragonite is replaced by calcite; HMC either dissolves or loses its Mg content. Traditional means of

recognising an aragonite precursor of diagenetic calcite rely on elevated levels of strontium (e.g. Sandberg 1983) and HMC precursors are generally characterised by associated microdolomite (Dickson 2001a, b). Both these proxies are limited as they allow detection of the original mineralogy only if diagenesis occurred in a semi-closed system that retained the freed Mg^{2+} and Sr^{2+}ions. More recently, the application of electron backscatter diffraction (EBSD) to biomineralised and geological materials has opened up a new approach to questions of biomineralisation, palaeontology, and $CaCO_3$ diagenesis (e.g. Cusack et al. 2008; Balthasar et al. 2011; Cusack 2016). EBSD provides information on the mineralogy and crystallographic orientation of individual grains with a potential submicronic resolution and thus can provide previously unavailable crucial information on the diagenetic history of rocks. Thus the application of EBSD provided here, to a variety of Palaeozoic stromatoporoids from various locations and a well-preserved chaetetid reference sample from the Pennsylvanian Buckhorn Asphalt Quarry (Oklahoma, USA), may help to explain the unique preservation of stromatoporoids, reconstruct the primary mineralogy of these sponges, and demonstrate striking similarities in the biomineralisation of Palaeozoic and modern hypercalcifying sponges.

Materials and Methods

Stromatoporoid samples were carefully selected to examine similarities and differences using EBSD analysis. One sample of each of two Silurian stromatoporoid taxa, *Petridiostroma simplex* (Nestor) and *Pachystroma hesslandi* (Mori) were collected from the same limestone and marl facies of the lowermost Wenlock of Gotland, Sweden, chosen because the Silurian was a time of abundance of stromatoporoids, and also because the marly facies tend to leave better preserved specimens. These two taxa have very different skeletal architectures (Fig. 1, d-g) allowing comparison of different stromatoporoid taxa subjected to the same environmental and diagenetic conditions (Mori 1969). *P. simplex* is constructed of prominent continuous horizontal elements called laminae, separated by approximately circular vertical pillars, thereby enclosing a system of galleries filled with cement (Fig. 1 d, e). Galleries are interpreted to have been occupied by soft tissue in the upper few millimetres of living sponge, but below the living layer, galleries were empty and later filled with calcium carbonate cement, as in modern hypercalcified sponges. *P. hesslandi* is composed of a reticulate network of micropillars and microlaminae (Fig. 1 f, g), in which distinct laminae and pillars are not present, so that gallery space comprises small areas within the fine network. Thus *P. hesslandi* possesses a much finer structure than *P. simplex;* however, at hand specimen scale, growth layering is visible in both taxa (Fig. 1 a, b). Astrorhizae (canals in the skeleton that carried exhalent tubes of the sponge, Stearn 2015a) are common in *Pachystroma* (faintly visible in Fig. 1g) but rare in *Petridiostroma*, in which the exhalant tubes most likely lay in the soft-tissue layer above the skeleton, so did not leave evidence in the skeleton itself.

The two Devonian stromatoporoids are *Stictostroma* (two samples, Fig. 1h, i) and *Atelodictyon* (one sample, Fig. 1j, k), collected from the same locality in reef facies in middle Frasnian limestones of southern Belgium described by Da Silva et al. (2011a, b). *Stictostroma* and *Atelodictyon* are both constructed of well-defined laminae and pillars with prominent gallery space. *Atelodictyon* has blade-like pillars often joined forming chains (Fig. 1k) contrasting the separate circular pillars of *Stictostroma* (Fig. 1i).

At a finer scale of construction, stromatoporoids also possess microstructural variations within the laminae and pillars. The microstructure of *Petridiostroma*, *Pachystroma* and *Atelodictyon* is termed compact in stromatoporoid terminology (Stearn 2015b), and is micritic, different from *Stictostroma* which possesses a cellular microstructure. Unfortunately, because of operational problems, EBSD images were not obtained from *Stictostroma*, so its difference in microstructure could not be investigated. However, BSE and elemental maps of *Stictostroma* were assembled and compared with the other specimens.

The chaetetid from the Pennsylvanian (Upper Moscovian) Buckhorn Asphalt Quarry (Oklahoma, USA; specimen BSPG 2011 X 16 in Seuss et al. [2014]) was included because of its remarkable preservation. Chaetetid sponge skeletons, including the sample studied here, are characterised by elongate tubules that appear as polygonal honeycombs in cross section (Fig. 1, l-n), with walls of 50-100 µm thick and a diameter of up to 500 µm (Figs. 2, 3; see West 2012). Because sediments of the Buckhorn Asphalt Quarry were impregnated by hydrocarbons prior to or at the time of lithification, there is excellent preservation of calcareous shells, including aragonite (Seuss et al. 2009). Chaetetids and stromatoporoids were likely both originally composed of fibrous bundles of calcium carbonate crystals, as explained later. This chaetetid (Fig. 1, l-m) therefore provides a reference sample to compare with the stromatoporoids. Chaetetids are composed of a calcium carbonate fibrous structure that is normally very well preserved, in contrast to the recrystallised structure of stromatoporoids. A well-preserved stromatoporoid would have been ideal as a reference sample, but such does not seem to exist in the rock record. The detailed discussion of stromatoporoid mineralogy and diagenesis by Stearn (2015b) explores their variation, but recognition of original structures remains uncertain. Justification for the use of the Buckhorn chaetetid may be found from a series of papers by Gilis et al. (2011, 2012, 2013) who studied the skeletal microstructure of the basal skeleton of a diverse set of extant hypercalcifying sponges. They found that, independent of taxonomy or skeletal structure and mineralogy, almost all species investigated secrete their skeletons extracellularly and form single-crystal fibres and crystal bundles composed of up to 100 nm large grains. Thus, a detailed study using EBSD patterns of the chaetetid microstructure, as the best material available, to compare with microstructure of stromatoporoids, is a valuable approach to advance understanding.

The chaetetid specimen was treated initially with the organic solvent methylene chloride (CH_2Cl_2) to remove asphalt from the specimen and then impregnated with araldite resin. Removal of the asphalt was important to avoid contamination of analytical instruments. The chaetetid and all stromatoporoid specimens were cut and polished down to 1 micron for backscatter scanning electron microscope (SEM) documentation. For EBSD analyses a FEI Quanta 200F field emission SEM equipped with an EDAX TSL Hikari high speed EBSD camera running Orientation Imaging Microscopy (OIM) software version 5.32 was used. Samples were highly polished (down to 0.06 µm) and coated with approximately 5 nm of carbon, then analysed in high vacuum mode with a beam aperture of 50 µm and an accelerating voltage of 20 kV. The Kikuchi patterns were indexed using the American Mineralogist Crystal Structure (AMCS) database to identify the mineralogy and crystallographic orientation at each point in the EBSD map. EBSD images of two types are shown in this study: a) grey-scale diffraction intensity maps showing the intensity of diffraction at each point of the imaged area, an assessment of the image quality (IQ) of the EBSD data; and b) colour-coded crystal orientation maps (see Fig.

3e for the colour key for orientation of calcite crystals). Both types are illustrated in this study, together with some combined maps to compare the diffraction intensity with crystal orientation, thus aiding understanding of the nature of the skeletal tissue.

The PaleoReefs Database (PARED) was accessed on 20th April 2017. All Palaeozoic stromatoporoids and entries of chaetetid-grade sponges were treated as calcitic. The PARED entries were assigned to the 10 million-year time bins of the Paleobiology Database (see Alroy et al. 2008).

Results

The chaetetid reference has excellent preservation in terms of microstructure and composition and is therefore presented first. Its fibrous microstructure provides important evidence for interpretation of the stromatoporoid skeletal structures that also have evidence of a fibrous nature.

Chaetetid microstructure

The skeletal wall of the sample studied here is speckled with small irregular pores and has an overall grainy appearance in SEM backscatter images (Fig. 2b). The centre of the tubules is filled by blocky calcite cements that are often partially dissolved along cleavage planes (Fig. 2a). In the case of the Buckhorn sample studied here, the cement infill of the tubules and the skeletal wall is separated by a distinct gap that can reach tens of microns in thickness (Figs. 2-3); however, chaetetids normally lack this gap (e.g. Fig. 3a). Elemental maps (Fig. 2) show that this gap contains concentrations of carbon, which probably represent remaining traces of the asphalt that permeated the rock. This gap is also enriched in magnesium and contains many distinct crystals of dolomite that are juxtaposed to the skeletal wall (see also Fig. 6 in Seuss et al. [2014]) and likely formed before the asphalt migrated through the rock. Seuss et al. (2014) reported that most other chaetetid specimens from the same locality also contain earlier calcite cements that pre-date the asphalt emplacement.

EBSD analysis shows that the chaetetid skeletal wall is composed of distinct clusters of small calcite crystals that share similar, but not identical crystallographic orientations within each cluster (Fig. 3c-e). Clusters of crystallographically similar crystals are around 50-150 microns in dimension and share irregular boundaries. Individual crystals are blocky to elongate in cross section, 1-5 µm wide, and fan out with the more blocky cross sections in the narrower parts of the clusters and the elongate cross sections in the wider parts (Fig. 3).

Stromatoporoid microstructure

All five stromatoporoid specimens investigated exhibit a prominent micro-porosity in their skeletal walls (Figs. 4-11). Pores vary from submicron to 8 µm in size, are irregular to elongate in shape and seem randomly distributed (Figs. 4b; 5b; 8a). In addition to the pores, small inclusions are common that appear dark grey or bright grey/white in backscatter images (e.g. Fig. 8a). Elemental maps provide evidence that many of the darker crystals are Mg-rich (e.g. Fig. 8c), probably dolomite. Although the majority of dolomite is of submicron size and only evident through elemental maps, occasional clusters of larger (up to 10 µm) dolomite crystals occur in one specimen (Fig. 4b, d). Elemental maps also show little presence of Fe and Sr in stromatoporoids (Figs. 4, 6, 8, 9), discussed later.

EBSD analysis of the stromatoporoid samples shows that the porous skeletal walls are now composed of blocky calcite crystals that are syntaxially extended into the adjacent galleries (Figs 5b, 10c, 11). Two of the three stromatoporoids analysed with EBSD (*Pachystroma* and *Atelodictyon*) show that the part of the crystal representing the skeletal wall contains multiple regions with lattice defects in which the crystallographic orientation is slightly different from the neighbouring part of the same crystal (Figs 7c, 10c, 11c). In contrast, those parts of a crystal that extend beyond the skeletal wall into the gallery lack such defects and show a homogenous crystallographic orientation (most easily seen in Fig. 10c). The third specimen (*Petridiostroma*) analysed with EBSD shows no defects in either portion of the crystal, but shows clear syntaxial extension of the skeletal walls (Fig. 5b).

Discussion

This study addresses two linked aspects: 1) original microstructure, and original mineralogy, of the calcified sponge skeletons; and 2) the implications of the sponge skeletal features in the debate of aragonite-calcite seas. Although linked, these two aspects are considered separately, for clarity.

As a prelude to the discussion, we briefly discuss the terminology of high-Mg calcite (HMC). HMC is conventionally defined as calcite containing more than 4 weight% Mg (e.g. Dickson 1991), but ultimately this threshold is arbitrary. The close association of dolomite with the skeletal walls of our stromatoporoid and chaetetid specimens leaves little doubt that the Mg contained in this dolomite was sourced from the skeletal walls. However, the concentration of Mg may not have exceeded the threshold of 4 weight%. So in this discussion we use the term HMC to indicate calcite that contained sufficient Mg to produce microdolomite inclusions, and LMC to indicate calcite that had such a low Mg content that microdolomite was not formed.

Original microstructure

The work of Gilis et al. (2011, 2012, 2013) on modern calcified sponges, noted earlier, provides an important link between modern and ancient representatives. The smallest building block of sponge skeletons has been interpreted to comprise submicronic grains of original amorphous calcium carbonate (ACC) (Gilis et al. 2013) composition. However, the *observed* fundamental crystallised unit consists of single crystals of only a few 100 nanometres width and several microns long, which are organised into larger bundles that grow from a single point (Gilis et al. 2013). Due to the fibrous crystal shape, neighbouring crystals fan out, growing away from the origin of the crystal bundle (Gilis et al. 2011, fig. 4; also our Fig. 12a). Because individual crystals can be expected to grow along the same crystallographic axes, each bundle should have a distinct crystallographic identity and sharp boundaries with neighbouring crystal bundles (Fig. 3c for chaetetid, see also model drawing in Fig. 12a,b). This model can be applied to a variety of extant taxa from both Calcarea and Demospongea and it is likely to represent a plesiomorphic (i.e. ancestral) character for skeletal secretion; it is thus used as a working hypothesis for the secretion of the Palaeozoic chaetetid and stromatoporoids investigated here. The only noticeable exception to an extracellular assemblage of crystal fibres is the modern demosponge *Astrosclera willeyana*, which uses digested bacterial remains to seed aragonite spherules that grow intracellularly (Jackson et al. 2010; Wörheide 1998). However, the unusual skeletal secretion of *A. willeyana* is interpreted to have been acquired by horizontal gene transfer from associated bacteria (Jackson et al. 2011) and is

unlikely to reflect a shared biomineralisation pathway for a larger taxonomic group of sponges.

The crystal fan model outlined above is consistent with the microstructure of the Buckhorn chaetetid (Fig. 3b-e), which shows distinct clusters of crystals with similar crystallographic orientation and shapes that can easily be visualised as a horizontal to oblique cross section through a fan of single-crystal fibres. However, with up to 5 µm in size, individual crystals in the chaetetid skeletal walls are much bigger and more irregular than those from extant sponges (Gilis et al. 2011, 2012, 2013). This difference can be attributed to the transformation from diagenetically unstable HMC to stable LMC via a micron-scale dissolution-precipitation process because the altered structure retains a fibrous character interpreted to reflect the pre-alteration crystal bundles. By comparison, in echinoderms, this process can preserve micron-scale microstructures while at the same time preserving micro-porosity and micro-dolomite within the space of the primary skeleton (Dickson 2001a, b). In echinoderms, the best preservation was observed when the stereom was filled by low magnesium ferroan calcite (Dickson 2004), evidence that entombment within stable low-magnesium calcite protected the less stable HMC of the echinoderm skeleton from diagenetic pore fluids. We interpret the asphalt impregnation of the Buckhorn chaetetid has effectively resulted in the same protection, because the apparent dissolution of calcite cement within the tubules has not noticeably affected the skeletal walls in the studied specimen.

For the stromatoporoids, their diagenesis resulted in coarse blocky calcite crystals with lattice defects. The defects are clearly constrained to the skeletal portion of crystals of those two taxa, whereas crystallographically homogenous regions occupy non-skeletal areas (i.e. galleries) of the structure. Presence of subcrystals with varying orientations in the skeletal parts of *Pachystroma* and *Atelodictyon* (Figs. 7, 10 and 11) are thus interpreted as diagenetic fusions and alteration of multiple individual crystals that originally had similar, but not identical crystallographic orientations. In diagenetic terms, single crystals with multiple internal crystallographic alignments are unstable and we interpret that they became crystallographically homogenous structures over time. However, there are some differences in the structure of the stromatoporoids. The specimen of *Petridiostroma* (Fig. 5) does not show the subtle variations in subcrystal orientations preserved in *Pachystroma* and *Atelodictyon*, for which we consider two possible interpretations: a) variations in diagenetic history between stromatoporoids; or b) [more likely] *Petridiostroma* was constructed differently from the other two taxa and lacked bundles of small crystals when it grew. *Petridiostroma* and *Pachystroma* occur together, sometimes in the same stromatoporoid specimen, where one overgrew the other, and were presumably affected by the same diagenetic processes. Although Stearn (2015b) noted that variation of stromatoporoid microstructure may relate to different processes of alteration, we consider a more likely scenario is that the diagenetic pathways were the same, but differing original structure of the stromatoporoid influenced the diagenetic result. These preliminary interpretations will require a larger sample of different taxa to investigate using EBSD. In *Pachystroma* and *Atelodictyon,* the shape and size of calcite crystals with domains of crystallographic misalignments in the stromatoporoid skeletal walls are very similar to the crystal bundles described for chaetetids above. We therefore view this similarity as evidence that the same principal biomineralisation sequence applies, i.e. based on the Gilis et al. (2011) model discussed above (also Fig. 12).

Original mineralogy

Diagenesis of echinoderm skeletons provides a valuable model for the recognition of original HMC composition in fossil skeletal material, outlined here for comparison with stromatoporoids. Experimental studies have shown that when heated up to 300° C, with and without added water, echinoid plates of HMC composition transform to calcite + dolomite together with a characteristic micro-porosity (Dickson 2001a). Importantly, these heating experiments showed that dolomite formation is a dissolution-precipitation process that depends on the availability of intra-skeletal water. The irregular distribution of the experimentally produced micropores is thus controlled by the distribution of water within the skeletal calcite. Molecular water is found in many calcifying organisms (Gaffey 1988), and in echinoderm skeletal plates it can make up to 3.38% of their weight (Gaffey 1995). The presence of water within calcareous skeletons is most likely linked to hydrated amorphous calcium carbonate ($ACC{\cdot}H_2O$) which in echinoderms forms the initial precursor of HMC (Politi et al. 2004). Although $ACC{\cdot}H_2O$ transforms via ACC to HMC in a matter of hours, nanometric traces of $ACC{\cdot}H_2O$ can survive within the mature calcite structure, probably due to stabilisation by proteins (Gong et al. 2012). Following this argument, the stability of $ACC{\cdot}H_2O$ within skeletal structures should be dependent on the stability of the relevant proteins. Although intra-skeletal proteins might not be stable over longer geological time scales (Marin et al. 2014), the preservation of such proteins in 1500-year old snails (Sarashina et al. 2008) is evidence that the water associated with skeletal $ACC{\cdot}H_2O$ becomes available in the course of early diagenesis. A critical point is that because fossil echinoderms from non-metamorphosed sedimentary rocks exhibit the same pattern of microporosity and dolomite as produced in experiments on modern echinoderms (Dickson 2001b), it is reasonable to interpret that the diagenetic pathways described are not dependent on excessive heating.

From the above discussion, diagenesis of the Buckhorn chaetetid and stromatoporoids is consistent with the presence of $ACC{\cdot}H_2O$ in their original mineralised skeleton. A role of ACC in skeletal secretion has so far been documented for only the calcite spicule formation of the calcarean genus *Clathrina* (Aizenberg et al. 1996; Sethmann & Wörheide 2008), but has also been interpreted to play a role in the formation of the basal skeletons of hypercalcifying sponges (Gilis et al. 2013), although direct evidence is still missing. In summary, the distinct preservation of the fossil sponges is consistent with a role of $ACC{\cdot}H_2O$ in the biomineralisation of Palaeozoic stromatoporoids and the Buckhorn chaetetid (Fig. 12).

Because both echinoderms and stromatoporoids retain evidence of primary structure in their altered states in fossil material, we interpret this comparability as evidence that crinoids found in the same samples as sponges investigated here were affected by the same diagenetic conditions. Both the chaetetid sample and stromatoporoids studied here exhibit the same pattern of microporosity and scattered distribution of dolomite (Figs. 2, 4, 8, 9), which provides a strong argument for original skeletal composition of HMC. This strengthens similar previous interpretations of the original HMC composition of stromatoporoids (e.g. Rush & Chafetz 1991; Yoo & Lee 1993) and the Buckhorn chaetetid (Seuss et al. 2014), which were based on the occurrence of dolomite alone. The alternative interpretations, of original LMC or aragonite skeletal composition, fail to explain all the observations. An original LMC composition is not consistent with the common occurrence of microporosity and finely scattered minute dolomite. Thus, the

interpretation by Stanley & Hardie (1998) that Palaeozoic stromatoporoids were originally LMC, and that Mg:Ca fluctuations drove the skeletal composition of dominant reef builders, is at odds with evidence presented in this study and in papers that propose a HMC composition (e.g. Rush & Chafetz 1991; Yoo & Lee 1993). Furthermore, an original aragonite composition is less likely because the orthorhombic aragonite structure makes it impossible for trigonal calcite to form syntaxial overgrowths that grow in crystallographic continuity. We note the very low levels of Sr in samples studied here (Figs. 4, 8, 9). The slightly raised concentrations of strontium (400-500 ppm) observed in one Devonian stromatoporoid specimen (Da Silva et al. 2014) are not a convincing argument for an original aragonite composition; in comparison with crinoids, concentrations of up to 1700 ppm strontium have been reported for HMC plates of echinoderms (Dickson 2001a, b). Finally, despite the argument for an original HMC composition of stromatoporoids, we note that in Stearn's (2015b) discussion of stromatoporoid mineralogy, he reported earlier studies where stromatoporoids did not contain dolomite. Thus, the link between occurrence of microdolomite inclusions and original HMC mineralogy of stromatoporoids, remains a hypothesis for which there is strong support but not proof.

Although this study focussed on only a few specimens, our results are consistent with the unusual preservation of Palaeozoic stromatoporoids characterised by coarse calcite crystals oriented normal to, and cutting across, horizontal galleries and vertical pillars (Kershaw 2013). As argued above, this preservation is inconsistent with an original aragonite composition. However, not all Palaeozoic stromatoporoids are preserved in this way. Semeniuk (1971), for example, described an Ordovician stromatoporoid, *Alleynodictyon*, which is preserved as a mouldic secondary calcite infill and thus might have been composed originally of aragonite. Mallamo and Stearn (1991) also interpreted aragonite for Ordovician stromatoporoids. Thus the interpretation here that Palaeozoic stromatoporoids had an original HMC composition may not apply to all of them.

Stromatoporoid mineralogy and the calcite-aragonite seas debate

Here we assess the relationship between stromatoporoid mineralogy and another aspect of the aragonite-calcite seas debate, that of temperature control on mineralisation. Because Mg^{2+} ions act as calcite-specific growth inhibitors, an increasing Mg:Ca ratio favours the precipitation of aragonite in non-biogenic settings (Morse et al. 2007). Phanerozoic oscillations in the Mg:Ca ratio broadly coincide with the original mineralogy of non-biogenic $CaCO_3$ precipitates and the composition of evaporites throughout the Phanerozoic (Sandberg 1983; Hardie 1996) and have thus been widely regarded as the main drivers of Phanerozoic aragonite-calcite sea conditions. However, experimental work has shown that whether non-biogenic $CaCO_3$ precipitation results in aragonite or calcite is strongly temperature dependent (Morse et al. 1997; Balthasar & Cusack 2015). Throughout the Phanerozoic Eon, this temperature effect on $CaCO_3$ polymorphs should have resulted in a much higher proportion of non-biogenic aragonite precipitation in shallow tropical seas than proposed from the traditional focus on the Mg:Ca ratio alone (Balthasar & Cusack 2015). Following Eichenseer et al. (2019), we combined the relationships between temperature, Mg:Ca ratio and the percentage of aragonite as described by Balthasar and Cusack (2015), with $\delta^{18}O$-based tropical shallow-water temperature estimates (Veizer & Prokoph 2015) and the Mg:Ca ratios modelled by Demicco et al. (2005) to create a measure of 'aragonite sea intensity' through time. We thus argue that non-

biogenic aragonite was likely to have fluctuated substantially throughout the Palaeozoic (Fig. 13). Particularly through the Ordovician-Devonian period this fluctuation was mainly driven by temperature as the Mg:Ca ratios remained at or slightly below 1 (Fig. 13).

Considering that, throughout their mid-Ordovician to Early Carboniferous stratigraphic range (Kershaw & Sendino 2020), the skeletal composition of Palaeozoic stromatoporoids is interpreted here to have been mainly HMC, it seems unlikely that temperature significantly influenced their skeletal mineralogy. In addition to stromatoporoids, it is useful to assess the skeletal composition of entire stromatoporoid-dominated reefs. To do this we considered sponge-dominated reefs in the PaleoReefs Database (PARED) (Fig. 13). The reef mineralogy in PARED is estimated based on the original mineralogy of the main reef builders of each individual reef (Kiessling et al. 2008) and thus shows that stromatoporoids were mainly associated with other calcitic reef builders in sponge-dominated Ordovician – Devonian reefs. The minor contributions of likely aragonitic organisms in these reefs are mainly due to fossils such as *Tetradium* and receptaculitids. Following the late Devonian mass extinction, sponge-dominated reefs were rare until the Late Permian but, where they are recorded, they are interpreted as having been dominated by originally aragonitic reef builders (Fig. 13).

Together, the data discussed above are presented as evidence that, contrary to the effect of temperature on non-biogenic $CaCO_3$ polymorph formation, the skeletal composition of Palaeozoic stromatoporoids was not noticeably influenced by temperature. The Mg:Ca ratio, on the other hand, shows a reasonably good correlation with the skeletal composition of stromatoporoids and with the mineral composition of Palaeozoic reefs dominated by hypercalcified sponges. It thus appears that the skeletal composition of Palaeozoic hypercalcifying sponges is influenced primarily by the Mg:Ca ratio instead of a combination of Mg:Ca ratio and temperature.

Finally we consider a caveat regarding the possible impact of biotic effects on sponge mineralisation separate from changes in global seawater. The above discussion is based on the notion that the Palaeozoic hypercalcified sponges precipitated calcium carbonate in equilibrium with contemporary seawater. However, Gaffey (1991, 1995) working on a range of living calcified organisms not including sponges, noted that because calcium carbonate skeletons are secreted within soft tissue, there is a barrier between skeleton formation sites and the external environment. This barrier breaks down when soft tissue decays and the skeletons come into contact with seawater, so the potential for very early diagenetic change to shift skeletal compositions is noted in modern organisms (Gaffey 1991). More recent work by Germer et al. (2015) and Garate et al. (2017) on non-hypercalcified sponges, identified bacterial control on precipitation of calcium carbonate spherules. The possible extent to which biological control of calcification can apply to Palaeozoic stromatoporoids and chaetetids cannot be assessed in this study, but may play a part in the reason why some stromatoporoid taxa produce a different skeletal structure from others (compare *Petridiostoma* and *Pachystroma* that occur together, discussed above). Thus, in conclusion, although we regard the Mg:Ca ratio was a key control on mineralogy of chaetetids and stromatoporoids, vital effects cannot be excluded.

Conclusions

1. A well-preserved Carboniferous chaetetid and examples of Silurian and Devonian stromatoporoids were examined using electron backscatter diffraction (EBSD). Observed microstructures are consistent with stromatoporoid skeletons having been composed originally of bundles of calcite crystals that were subsequently altered, yet retain remnant evidence of crystal bundles in the subtle variations of crystal orientations within the altered structure.
2. Presence of microdolomite within stromatoporoid partially-preserved skeletal structures is evidence of an original high-Mg calcite composition. These results are consistent with other interpretations reported in the literature.
3. Stromatoporoids flourished during a time of stable seawater Mg:Ca ratios but significant temperature variability. The low amounts of aragonite in stromatoporoid-dominated reefs throughout the Ordovician – Devonian is interpreted to indicate that the composition of these reefs was not noticeably impacted by temperature fluctuation but is consistent with an influence of the Mg:Ca ratio on the skeletal mineralogy of these reef types.

Acknowledgments

We are grateful for the use of the facilities of the Imaging Spectroscopy & Analysis Centre (ISAAC), School of Geographical & Earth Sciences, University of Glasgow. We also thank Mrs Heltzel for access to her private property to access the Buckhorn Asphalt Quarry. Ronald West (Kansas) facilitated collection and processing of sample illustrated in Fig. 3A. We thank Juwan Jeon (Nanjing) and Chelsea Pederson (Bochum) for careful reviews of the manuscript.

Declarations

Funding: BS was supported by funding from the DFG (NU 96/10-1, 2 und SE 2283/2-1). MC gratefully acknowledges support of the Natural Environment Research Council (NE/P011063/1). ACDS Acknowledges the National Science Foundation program (FNRS) for financial support (T.0051.19). KE was supported by a doctoral studentship by the University of Plymouth.

Conflicts of interest/Competing interests: there are no conflicts or competing interests associated with this study.

Code availability: not applicable.

Availability of data and material (data transparency).

Authors' contributions: UB, MC, KE and PC did the analyses; UB, SK, ACD, MC and BS wrote the paper.

References

Aizenberg J, Lambert G, Addadi L, Weiner S (1996) Stabilization of amorphous calcium carbonate by specialized macromolecules in biological and synthetic precipitates. *Advanced Materials* 8: 222–226. DOI: 10.1002/adma.19960080307

Alroy J, Aberhan M, Bottjer DJ, Foote M, Fürsich FT, Harries PJ, Hendy AJW, Holland SM, Ivany LC, Kiessling W, Kosnik MA, Marshall CR, McGowan AJ, Miller AI, Olszewski TD, Patzkowsky ME, Peters SE, Villier L, Wagner PJ, Bonuso N, Borkow PS, Brenneis B, Clapham ME, Fall LM, Ferguson CA, Hanson VL, Krug AZ, Layou KM, Leckey EH, Nürnberg S, Powers CM, Sessa, CA, Simpson C, Tomašových A, Visaggi CC (2008) Phanerozoic trends in the global diversity of marine invertebrates. Science 321: 97-100

607 Balthasar U, Cusack M (2015) Aragonite-calcite seas-Quantifying the gray area.
608 Geology 43: 99-102. DOI: 10.1130/G36293.1
609 Balthasar U, Cusack M, Faryma L, Chung P, Holmer LE, Jin J, Percival IG, Popov
610 LE (2011) Relic aragonite from Ordovician-Silurian brachiopods: Implications
611 for the evolution of calcification. Geology, 39: 967-970. DOI: 10.1130/G32269.1
612 Cusack M, England J, Dalbeck. P, Tudhope AW, Fallick AE (2008) Electron
613 backscatter diffraction (EBSD) as a tool for detection of coral diagenesis. Coral
614 Reefs 27: 905-911. DOI: 10.1007/s00338-008-0414-3.
615 Cusack M (2016) Biomineral electron backscatter diffraction for palaeontology.
616 Palaeontology 59: 171-179. DOI: 10.1111/pala.12222
617 Da Silva AC, Kershaw S, Boulvain F (2011a) Stromatoporoid palaeoecology in the
618 Frasnian (Upper Devonian) Belgian platform, and its applications in
619 interpretation of carbonate platform environments. Palaeontology 54: 883-905.
620 DOI: 10.1111/j.1475-4983.2011.01037.x
621 Da Silva AC, Kershaw S, Boulvain F (2011b) Sedimentology and stromatoporoid
622 palaeoecology of Frasnian (Upper Devonian) carbonate mounds in southern
623 Belgium. Lethaia 44: 255-274. DOI: 10.1111/j.1502-3931.2010.00240.x
624 Da Silva AC, Kershaw S, Boulvain F, Hubert BLM, Mistiaen B, Reynolds A, Reitner J
625 (2014) Indigenous demosponge spicules in a Late Devonian stromatoporoid
626 basal skeleton from the Frasnian of Belgium. Lethaia 47: 365-375. DOI:
627 10.1111/let.12064
628 Demicco RV, Lowenstein TK, Hardie LA, Spencer RJ (2005) Model of seawater
629 composition for the Phanerozoic. Geology 33: 877-880. DOI:
630 10.1130/G21945.1.
631 Dickson JAD (1991) Carbonate mineralogy and chemistry. pp. 284-313, In: Tucker
632 ME and Wright VP (eds): Carbonate Sedimentology. 498 pages, Blackwell
633 Science Ltd. Oxford. ISBN 978-0-632-01472-9
634 Dickson JAD (2001a) Transformation of echinoid Mg calcite skeletons by heating.
635 Geochimica et Cosmochimica Acta 65: 443-454. DOI: 10.1016/S0016-
636 7037(00)00547-0
637 Dickson JAD (2001b) Diagenesis and crystal caskets: Echinoderm Mg calcite
638 transformation, Dry Canyon, New Mexico, USA. Journal of Sedimentary
639 Research 71: 764-777. DOI: 10.1306/2DC40966-0E47-11D7-
640 8643000102C1865D
641 Dickson JAD (2004) Echinoderm skeletal preservation: calcite-aragonite seas and
642 the Mg/Ca ratio of Phanerozoic oceans. Journal of Sedimentary Research
643 74:355-365
644 Ehrlich H, Simon P, Carrillo-Cabrera W, Bazhenov V, Botting JP, Ilan M, Ereskovsky
645 AV, Muricy G, Worch H, Mensch A, Born R, Springer A, Kummer K, Vyalikh
646 DV, Molodtsov, S. L., Kurek, D., Kammer, M., Paasch, S., & Brunner, E. (2010).
647 Insights into Chemistry of Biological Materials: Newly Discovered Silica-
648 Aragonite-Chitin Biocomposites in Demosponges. *Chemistry of Materials*, **22**,
649 1462–1471; DOI:10.1021/cm9026607
650 Eichenseer, K, Balthasar, U, Smart, C, Stander, J, Haaga, K, Kiessling, W (2019)
651 Jurassic shift from abiotic to biotic control on marine ecological success. Nature
652 Geoscience 12: 638–642
653 Ehrlich H, Brunner E, Simon P, Bazhenov VV, Botting JP, Tabachnick KR, Springer
654 A, Kummer K, Vyalikh DV, Molodtsov SL, Kurek D, Kammer M, Born R,
655 Kovalev A, Gorb SN, Koutsoukos PG, Summers A (2011) Calcite Reinforced

656 Silica–Silica Joints in the Biocomposite Skeleton of Deep-Sea Glass Sponges.
657 Advanced Functional Materials 21: 3473–3481. DOI: 10.1002/adfm.201100749
658 Gaffey SJ (1988) Water in skeletal carbonates. Journal of Sedimentary Petrology 58:
659 397-414
660 Gaffey S (1991) Skeletal carbonate diversity: implications for marine diagenesis. In
661 Bain, R.J. (Ed.). Proceedings of the Fifth Symposium on the Geology of the
662 Bahamas. Bahamian Field Station, San Salvador, Bahamas. ISBN 0-935909-37-
663 0
664 Gaffey SJ (1995) H_2O and OH in echinoid calcite – a spectroscopic study. American
665 Mineralogist 80: 947-959
666 Garate L, Sureda J, Agell G, Uriz, MJ (2017) Endosymbiotic calcifying bacteria
667 across sponge species and oceans. Scientific Reports 7: 43674, DOI:
668 10.1038/srep43674.
669 Germer J, Mann K, Wörheide G, Jackson DJ (2015) The skeleton forming proteome
670 of an early branching metazoan: a molecular survey of the biomineralization
671 components employed by the coralline sponge *Vaceletia* sp. PLOS One 10(11):
672 e0140100. doi:10.1371/journal.pone.0140100.
673 Gilis M, Grauby O, Willenz P, Dubois P, Legras L, Heresanu V, Baronnet A (2011)
674 Multi-scale mineralogical characterization of the hypercalcified sponge
675 *Petrobiona massiliana* (Calcarea, Calcaronea). Journal of Structural Biology
676 176: 315–329. doi:10.1016/j.jsb.2011.08.008
677 Gilis M, Baronnet A, Dubois Ph, Legras L, Grauby O, Willenz P (2012) Biologically
678 controlled mineralization in the hypercalcified sponge *Petrobiona massiliana*
679 (Calcarea, Calcaronea). Journal of Structural Biology 178: 279–289. DOI:
680 10.1016/j.jsb.2012.04.004
681 Gilis M, Grauby O, Willenz P, Dubois P, Heresanu V, Baronnet A (2013)
682 Biomineralization in living hypercalcified demosponges: Toward a shared
683 mechanism? Journal of Structural Biology 183: 441–454. DOI:
684 10.1016/j.jsb.2013.05.018
685 Gong YUT, Killiana CE, Olsona IC, Appathuraic NP, Amasinoa AL, Martin MC, Holt
686 LJ, Wilt FH, Gilbert PUPA (2012) Phase transitions in biogenic amorphous
687 calcium carbonate. PNAS 109: 6088–6093. DOI: 10.1073/pnas.1118085109
688 Hardie LA (1996) Secular variation in seawater chemistry: An explanation for the
689 coupled secular variation in the mineralogies of marine limestones and potash
690 evaporites over the past 600 m.y. Geology 24: 279-283.
691 Jackson DJ, Thiel V, Wörheide G (2010). An evolutionary fast-track to
692 biocalcification. Geobiology 8: 191–196; DOI: 10.1111/j.1472-
693 4669.2010.00236.x
694 Jackson DJ, Macis L, Reitner J, Wörheide G (2011) A horizontal gene transfer
695 supported the evolution of an early metazoan biomineralization strategy. BMC
696 Evolutionary Biology 11: article number 238. DOI: 10.1186/1471-2148-11-238
697 Kershaw S (2013) Palaeozoic stromatoporoid futures: A discussion of their
698 taxonomy, mineralogy and applications in palaeoecology and
699 palaeoenvironmental analysis. Journal of Palaeogeography 2: 163-182.
700 DOI:10.3724/SP.J.1261.2013.00024
701 Kershaw S, Sendino, C (2020) Labechia carbonaria Smith 1932 in the Early
702 Carboniferous of England; affinity, palaeogeographic position and implications
703 for the geological history of stromatoporoid-type sponges. Journal of
704 Palaeogeography 9, https://doi.org/10.1186/s42501-020-00077-7

Kiessling W, Aberhan M, Villier L (2008) Phanerozoic trends in skeletal mineralogy driven by mass extinctions. Nature Geoscience 1: 527-530
Kiessling W, (2015) Fuzzy seas. Geology 43: 191-192. doi:10.1130/focus022015.1
Mallamo MP, Stearn CW (1991) Skeletal mineralogy of Ordovician stromatoporoids: New geochemical evidence for an aragonite skeleton. Geological Society of America, Abstracts with Programs 23**:** 164.
Manuel M, Borchiellini C, Alivon E, Boury-Esnault N (2004) Molecular phylogeny of calcareous sponges using 18S rRNA and 28S rRNA sequences. Bolletino dei Musei e degli Istituti Biologici dell' Universita Genova 68: 449–461
Marin F, Le Roy N, Marie B, Ramos-Silva P, Bundeleva I, Guichard N, Immel F (2014) Metazoan calcium carbonate biomineralizations: macroevolutionary trends - challenges for the coming decade. Bulletin de la Societe Geologique de France 185: 217-232
Mori K (1969) Stromatoporoids from the Silurian of Gotland I. Stockholm Contributions in Geology 19: 1-100
Morrow C, Cárdenas P (2015) Proposal for a revised classification of the Demospongiae (Porifera). Frontiers in Zoology 12: article number 7. DOI: 10.1186/s12983-015-0099-8
Morse JW, Wang Q, Tsio MY (1997) Influences of temperature and Mg:Ca ratio on $CaCO_3$ precipitates from seawater. Geology 25: 85-87
Morse JW, Arvidson RS, Lüttge A (2007) Calcium carbonate formation and dissolution. Chemical Reviews 107: 342-381
Politi Y, Arad T, Klein E, Weiner S, Addadi L (2004) Sea urchin spine calcite forms via a transient amorphous calcium carbonate phase. Science 306: 1161-1164. DOI: 10.1126/science.1102289
Rush PF, Chafetz HS (1991) Skeletal mineralogy of Devonian stromatoporoids. Journal of Sedimentary Petrology 61: 364-369
Sandberg PA (1983) An oscillating trend in Phanerozoic non-skeletal carbonate mineralogy. Nature 305: 19-22
Sarashina I, Kunitomo Y, Iijima M, Chiba S, Endo K (2008) Preservation of the shell matrix protein dermatopontin in 1500 year old land snail fossils from the Bonin islands. Organic Geochemistry 39: 1742-1746. DOI: 10.1016/j.orggeochem.2008.08.004
Semeniuk V (1971) Subaerial leaching in the limestones of the Bowan Park Group (Ordovician) of central western New South Wales. Journal of Sedimentary Petrology 41: 939-950
Sethmann I, Wörheide G (2008) Structure and composition of calcareous sponge spicules: A review and comparison to structurally related biominerals. Micron 39**:** 209–228. DOI: 10.1016/j.micron.2007.01.006
Seuss B, Senowbari-Daryan B, Nützel A, Dittrich S, Neubauer J (2014) A chaetetid sponge assemblage from the Desmoinesian (Upper Moscovian) Buckhorn Asphalt Quarry Lagerstätte in Oklahoma, USA. Rivista Italiana di Paleontologia e Stratigrafia 120: 3-26
Seuss B, Nützel A, Mapes RH, Yancey TE (2009) Facies and fauna of the Pennsylvanian Buckhorn Asphalt Quarry deposit: a review and new data on an important Palaeozoic fossil Lagerstatte with aragonite preservation. Facies 55: 609-645. DOI: 10.1007/s10347-009-0181-9
Smith AM, Berman J, Key MM Jr, Winter DJ (2013) Not all sponges will thrive in a high-CO_2 ocean: Review of the mineralogy of calcifying sponges.

Palaeogeography, Palaeoclimatology, Palaeoecology 392: 463–472. DOI: 10.1016/j.palaeo.2013.10.004
Stanley SM, Hardie LA (1998) Secular oscillations in the carbonate mineralogy of reef-building and sediment-producing organisms driven by tectonically forced shifts in seawater chemistry. Palaeogeography Palaeoclimatology Palaeoecology 144: 3-19
Stearn CW (2015a) Functional morphology of the Paleozoic stromatoporoid skeleton. Pp 551-573 In Selden, P. A., ed. 2015. Treatise on Invertebrate Paleontology. Part E (Revised), Porifera, vol. 4–5. The University of Kansas Paleontological Institute. Lawrence, Kansas. liii + 1223 p., 665 fig., 42 tables
Stearn CW (2015b) Microstructure and mineralogy of Paleozoic Stromatoporoidea. Pp 521-542 In Selden, P. A., ed. 2015. Treatise on Invertebrate Paleontology. Part E (Revised), Porifera, vol. 4–5. The University of Kansas Paleontological Institute. Lawrence, Kansas. liii + 1223 p., 665 fig., 42 tables
Stearn CW, Mah AJ (1987) Skeletal microstructure of Paleozoic stromatoporoids and its mineralogical implications. Palaios 2: 76-84
Uriz M-J (2006) Mineral skeletogenesis in sponges. Canadian Journal of Zoology 84: 322–356
Veizer J, Prokoph A (2015) Temperatures and oxygen isotopic composition of Phanerozoic oceans. Earth Science Reviews 146: 92-104. DOI: 10.1016/j.earscirev.2015.03.008
Voigt O, Wülfing E, Wörheide G (2012) Molecular phylogenetic evaluation of classification and scenarios of character evolution in calcareous sponges (Porifera, Class Calcarea). PLoS ONE 7: 1-16, article number e33417. doi:10.1371/journal.pone.0033417
Webby, BD (2015) Glossary of terms applied to the hypercalcified Porifera. Pp 397-416 In Selden, P. A., ed. 2015. Treatise on Invertebrate Paleontology. Part E (Revised), Porifera, vol. 4–5. The University of Kansas Paleontological Institute. Lawrence, Kansas. liii + 1223 p., 665 fig., 42 tables
West RR (2012) Evolution of the Hypercalcified Chaetetid-Type Porifera (Demospongiae). Treatise Online 35:1–26
Wörheide G (1998) The reef cave dwelling ultraconservative coralline demosponge *Astrosclera willeyana* Lister 1900 from the Indo-Pacific—Micromorphology, ultrastructure, biocalcification, isotope record, taxonomy, biogeography, phylogeny. Facies 38: 1–88
Wood R (1987) Biology and revised systematics of some late Mesozoic stromatoporoids. Special Papers in Palaeontology 37: 1-89
Yoo CM, Lee YI, (1993) Original mineralogy of stromatoporoids. Carbonates and Evaporites 8: 224-229

FIGURES

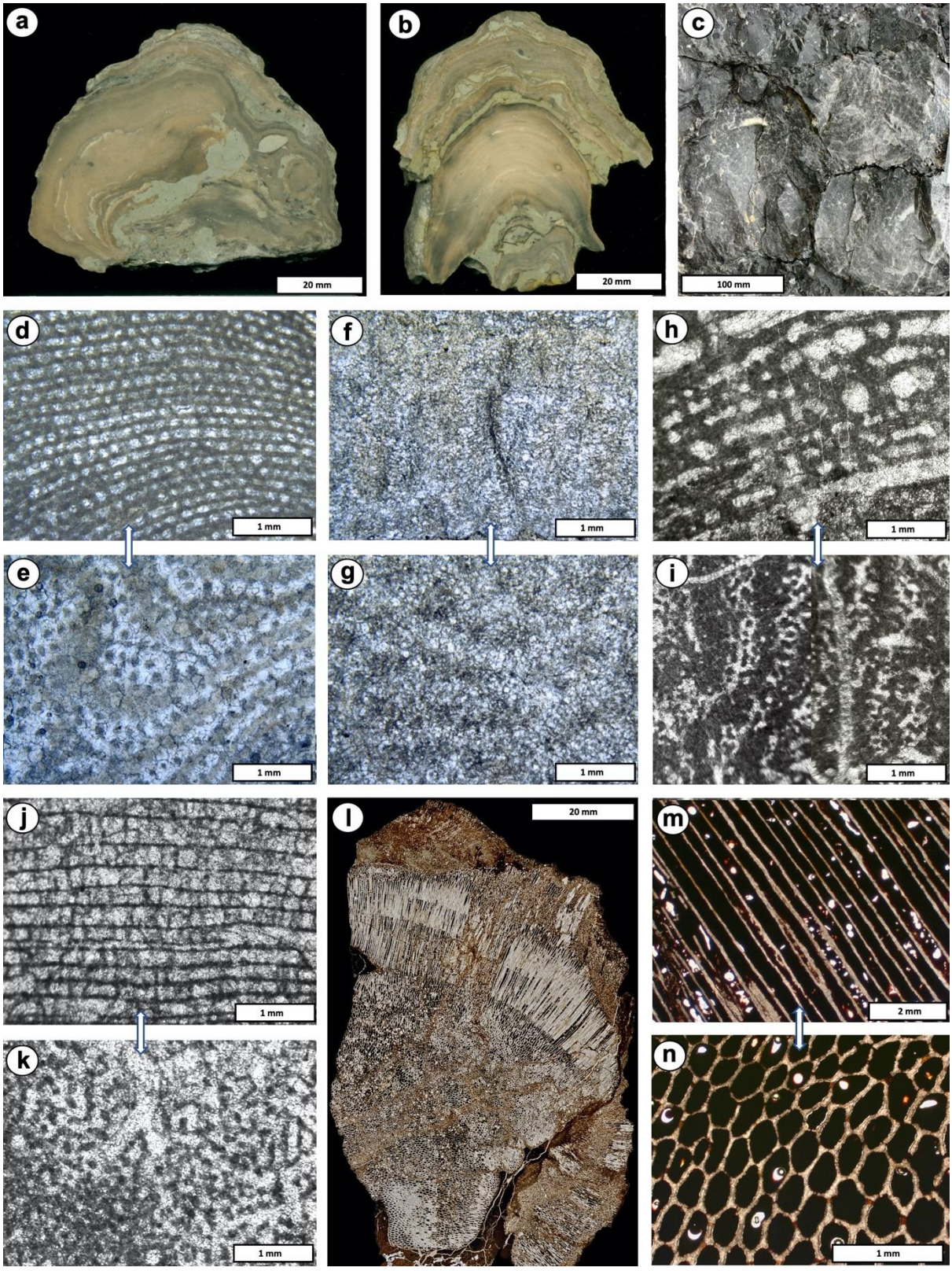

Fig. 1 Representative hand specimen and thin section (VS: vertical; TS: transverse) images of stromatoporoid and chaetetid taxa used in this study. **a** and **b** Domical stromatoporoid hand specimens in vertical section, including *Petridiostroma simplex* and *Pachystroma hesslandi*, Upper Visby Formation, Lower Wenlock, Silurian, of Gotland, Sweden; **c** Stromatoporoid field views in vertical section, Moulin Liénaux Formation, middle Frasnian, Upper Devonian of La Boverie Quarry, Belgium; **d** and **e**

Vertical (VS, d) and transverse (TS, e) thin section views of *Petridiostroma simplex*, Gotland; **f** and **g** VS (f) and TS (g) thin section views of *Pachystroma hesslandi*, Gotland; **h** and **i** VS (h) and TS (i) thin section views of *Stictostroma*, Belgium.; **j** and **k** VS (j) and TS (k) thin section views of *Atelodictyon*, Belgium; **l** Chaetetid whole thin section from the Buckhorn Asphalt Quarry, upper Moscovian Stage, Middle Pennsylvanian, Oklahoma, USA, after Seuss et al. (2009); **m** and **n** VS(m) and TS(n) enlarged thin section views of chaetetid from Buckhorn Quarry, Oklahoma, after Seuss et al. (2009). m is sample BSPG 2011 X 20a; n and o are samples BSPG 2011 X 18c stored in Bayerische Staatssamlung für Paläontologie und Geologie, Munich

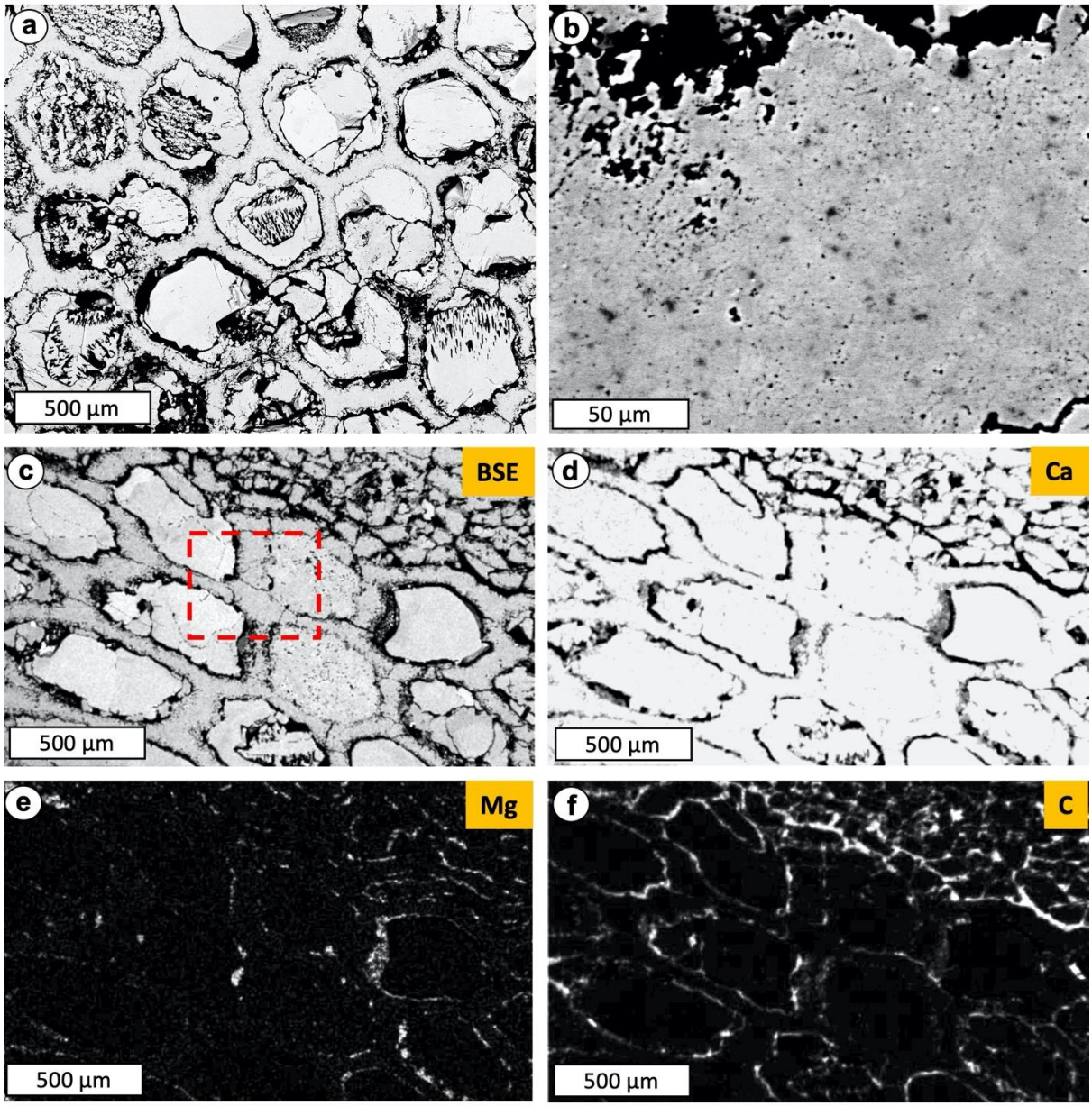

Fig. 2 Buckhorn chaetetid detailed structure. **a** BSE-image showing the characteristic polygonal tubule cross sections filled with partially dissolved cements; **b** BSE close-up of a skeletal wall showing the speckled appearance and microporosity; **c** BSE image; red box shows the area of EBSD map shown in figure 3; **d-e** elemental maps of Ca, Mg, and C of same area of **c**; in each case lighter tones represent higher concentrations of each element. Note that the stretched appearance of the chaetetid

in c-f is because the sample is tilted to 70 degrees for EBSD scatter image acquisition, although this is an orthogonal TS view. Note this issue affects all the BSE and EBSD images in this paper

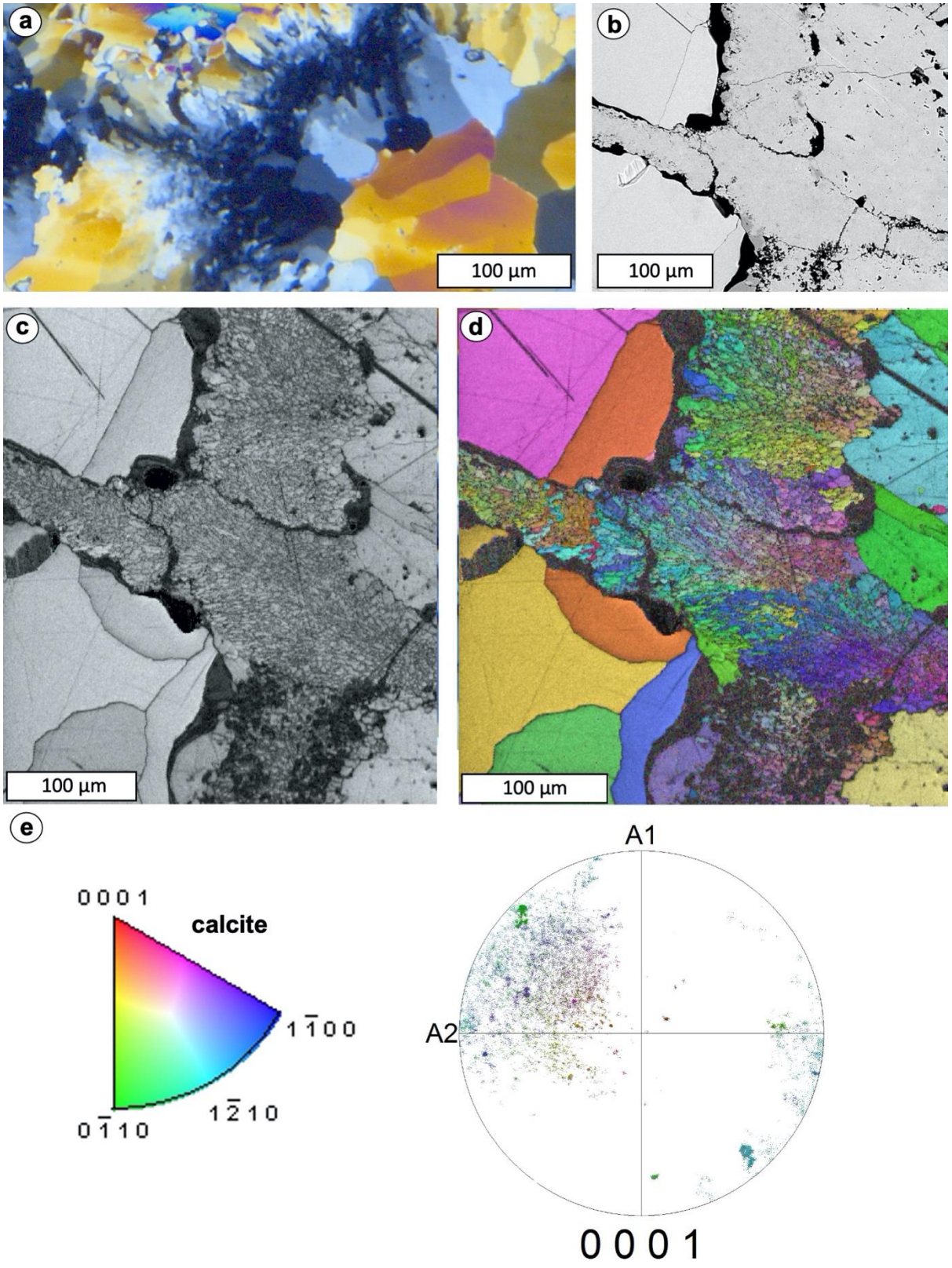

Fig. 3 Images of chaetetids. **a** Transverse ultrathin section in cross-polarised light, of chaetetid from a quarry in the Amoret Member of Altamont Limestone Formation, Pennsylvanian subsystem, near Coffeyville, Labette County, Kansas, showing transverse fibrous crystal structure in the walls. Note variation of extinction in neighbouring crystals reflecting the fibrous structure even though it is partially altered. This sample is provided for comparison with BSE and EBSD images, in the

absence of similar thin sections of the Buckhorn sample. **b** BSE image, of the Buckhorn chaetetid, of the area shown in red box in Fig. 2c, showing clear distinction between calicle wall and cavity-filling sparite. Prominent major crystal boundaries in the chaetetid skeletal wall indicate overprinting by recrystallisation of its structure (for example the sharp change from purple-blue to green-yellow in the centre of the image). **c** EBSD diffraction intensity map of same area as b. This shows that variation of intensity of diffraction from different crystals within the chaetetid wall is small except in the bottom centre of the image, where the dark shades reflect low reliability of information of crystal orientation. **d** combined diffraction intensity and crystal orientation map showing good quality of orientation information across most of the image. The same is true for the cement filling the calicles. The chaetetid skeletal wall shows a sharp boundary with the calicle fill sparite, contrasting the partly recrystallised thin section view in a, in a different sample from a non-lagerstätte deposit. Compare this image with stromatoporoid EBSD images illustrated in Figs 5, 7, 10 and 11; **e** (left diagram) colour code for crystal axes in the EBSD map of d; and (right diagram) crystal orientation pole diagram, showing clustered crystal orientations consistent with a fibrous skeletal structure, discussed in the text

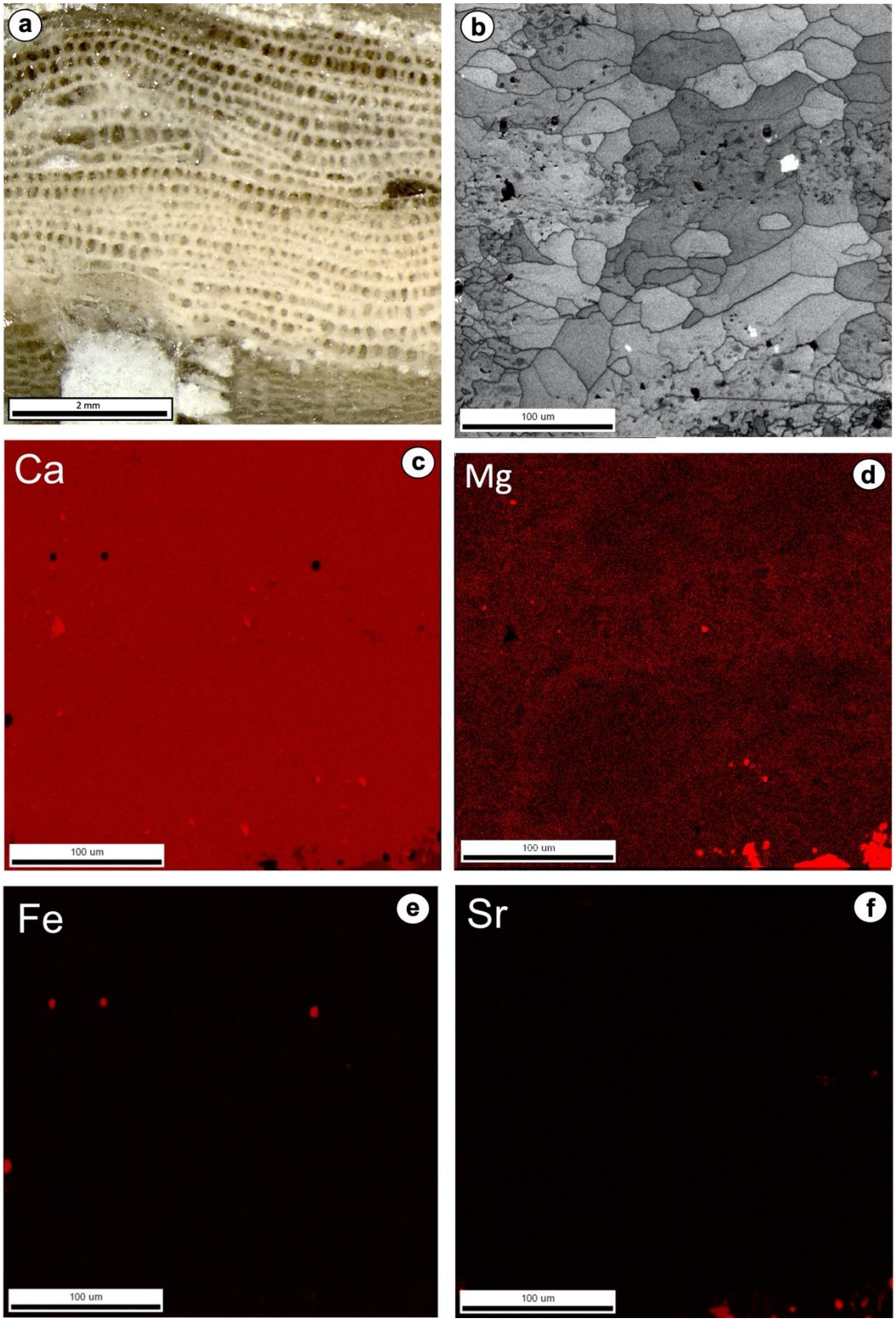

Fig. 4 *Petridiostroma simplex*, Silurian of Gotland, structure and elemental composition. **a** Vertical section of hand specimen showing laminae and pillars of a specimen that grew on top of a heliolitid tabulate after death of the tabulate, indicated by sediment in corallites. Dark areas between laminae and pillars are gallery spaces filled with sparite. **b** Diffraction intensity EBSD image emphasising the stromatoporoid skeletal structure composed of a speckled fabric overprinted by

diagenetic cement that passes into the gallery spaces. Two laminae (centre and bottom), most of one pillar (left) and part of another pillar (right) are illustrated, for comparison with a. The variation in grey shade between crystals corresponds to the intensity of diffraction from the sample surface; some crystals show less intensity but there is no difference in diffraction quality between the skeletal tissue and gallery cement in any crystal, likely indicating they have the same composition. **c-f** Elemental maps of the same area as b; in each case lighter tones represent higher concentrations of each element. Maps of Ca, Mg, Fe and Sr show there is very little difference between the skeletal walls and the gallery cements, typical of stromatoporoids, and discussed in the text. Levels of Sr and Fe are very low

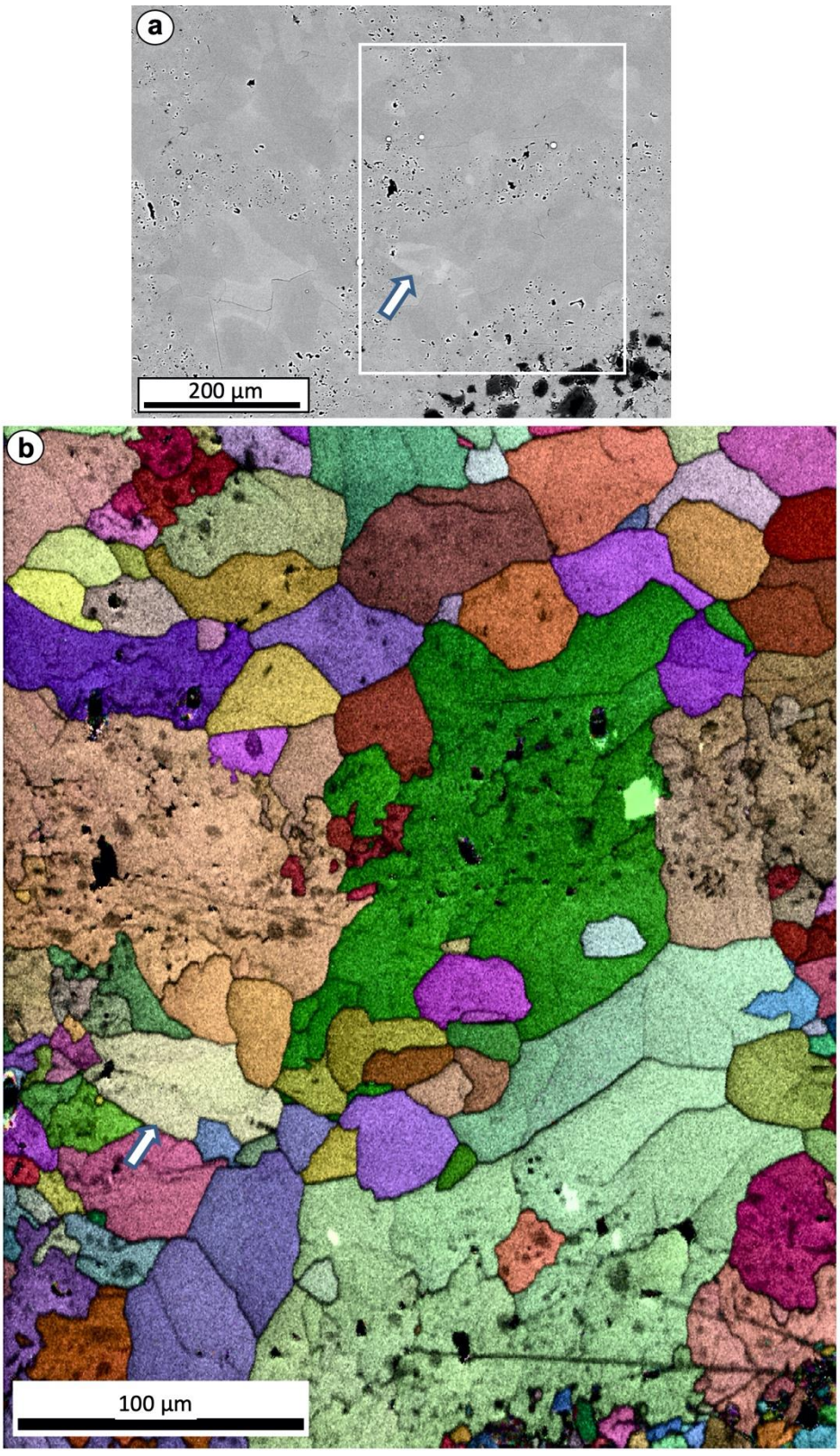

Fig. 5. *Petridiostroma simplex*, Gotland, skeletal structure. **a** BSE image of sample processed in this study showing faint speckled skeletal structure contrasting the gallery sparite. **b** Combined diffraction intensity and crystal orientation EBSD map of the white rectangle in b (that also represents the area of Fig. 4b), showing colour variation representing different orientations of calcite crystals passing between skeleton and gallery sparite. Skeleton of stromatoporoid is clearly distinguishable

from the sparite cement and shows the relatively sharp edge of the skeletal structure. Diffraction intensity varies between crystals but not between the skeletal tissue and gallery cement, likely indicating similar compositions of both. White arrow in b and c mark the same location in the two images

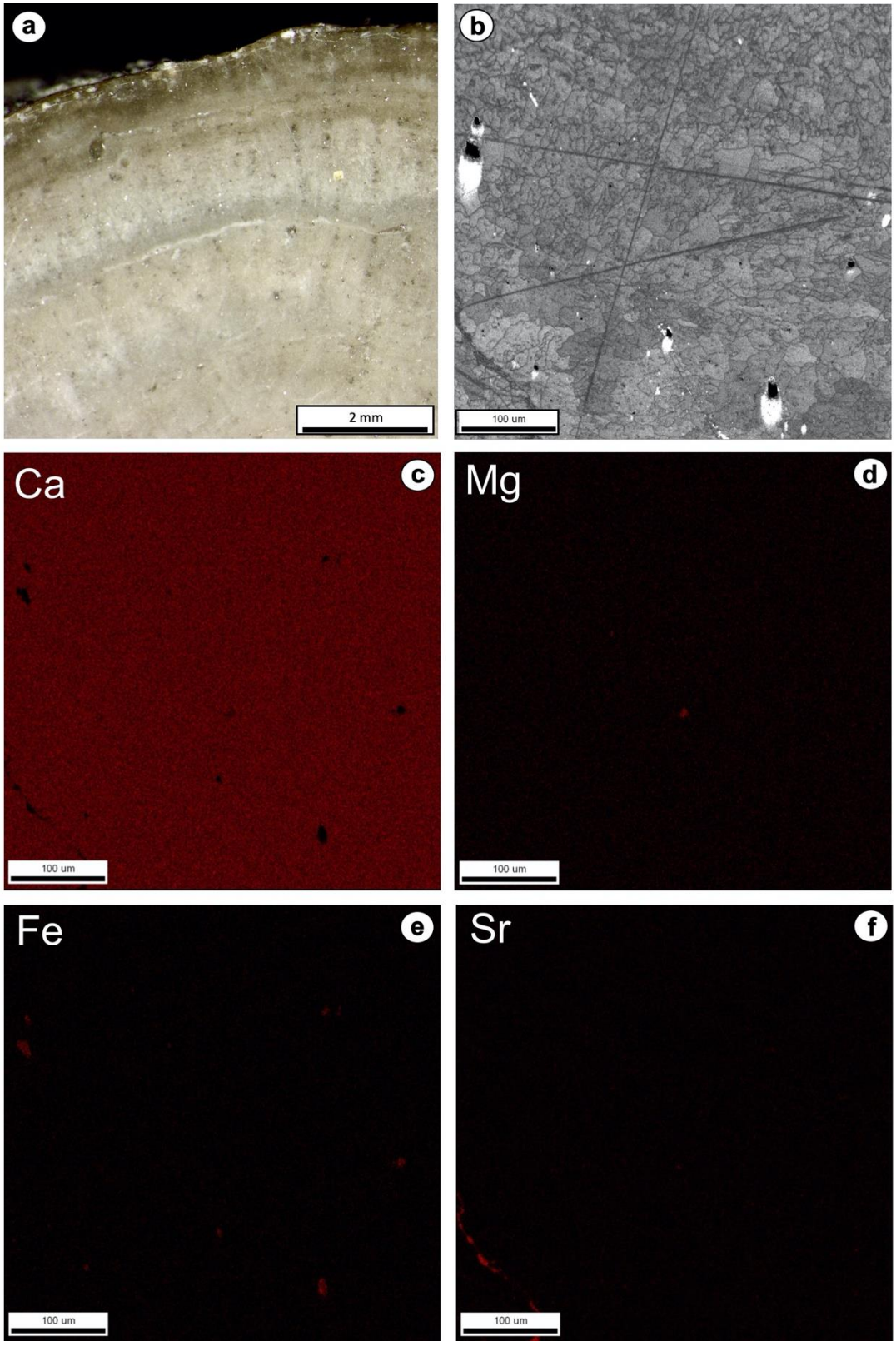

Fig. 6. *Pachystroma hesslandi*, Silurian of Gotland, structure and elemental composition. **a** Vertical section of hand specimen used in this study showing difference between the skeletal architecture of this taxon and that of *Petridiostroma simplex* illustrated in Figs. 1, 4 and 5; *P. hesslandi* lacks an obvious laminae and pillar arrangement, its skeleton being composed of a finer-structured fabric. **b** Diffraction intensity EBSD map reflecting the fine skeletal structure so that skeletal

component and gallery space are not as easily recognisable in this taxon as in *P. simplex*. Little variation in diffraction intensity between crystals is visible indicating reliable EBSD orientation data. **c-f** Elemental maps of the same area as b; in each case lighter tones represent higher concentrations of each element. Maps of Ca, Mg, Fe and Sr may be compared with those of *P. simplex* in Fig. 4; in both taxa there is very little difference in the elemental composition between the skeleton and cements in stromatoporoids

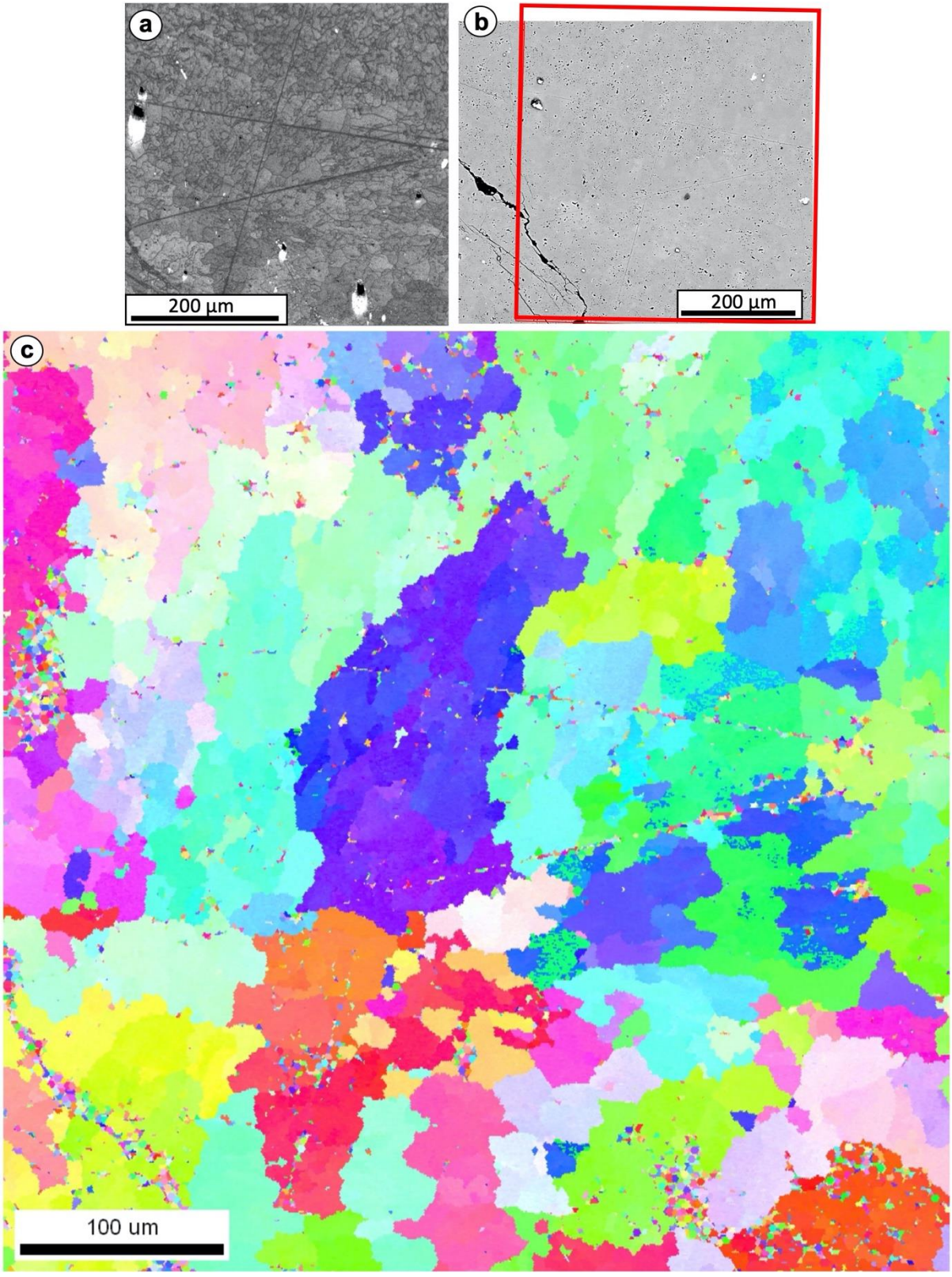

Fig. 7. *Pachystroma hesslandi*, Gotland, skeletal structure. **a** Repeat of diffraction intensity EBSD map in Fig. 6b to aid understanding of the areas in Figs. 7b and c. **b** BSE image of sample processed in this study showing the speckled skeletal structure occurs throughout the image in contrast to *P. simplex* (Fig. 5b). Thus in this taxon, the skeletal structure and gallery space are poorly distinguishable in b. **c** EBSD image of the area of the red box in b and the whole area of a. Colour variation

reflects crystal orientation. Note the contrast with *P. simplex* in Fig. 5, that has a more equant crystal structure, with less vertical elongation of crystals than in *P. hesslandi*. Note also the subtle colour shade changes within crystals illustrating shifts of crystal axes within the areas of larger crystals, that are interpreted to represent altered crystal bundles, discussed in the text

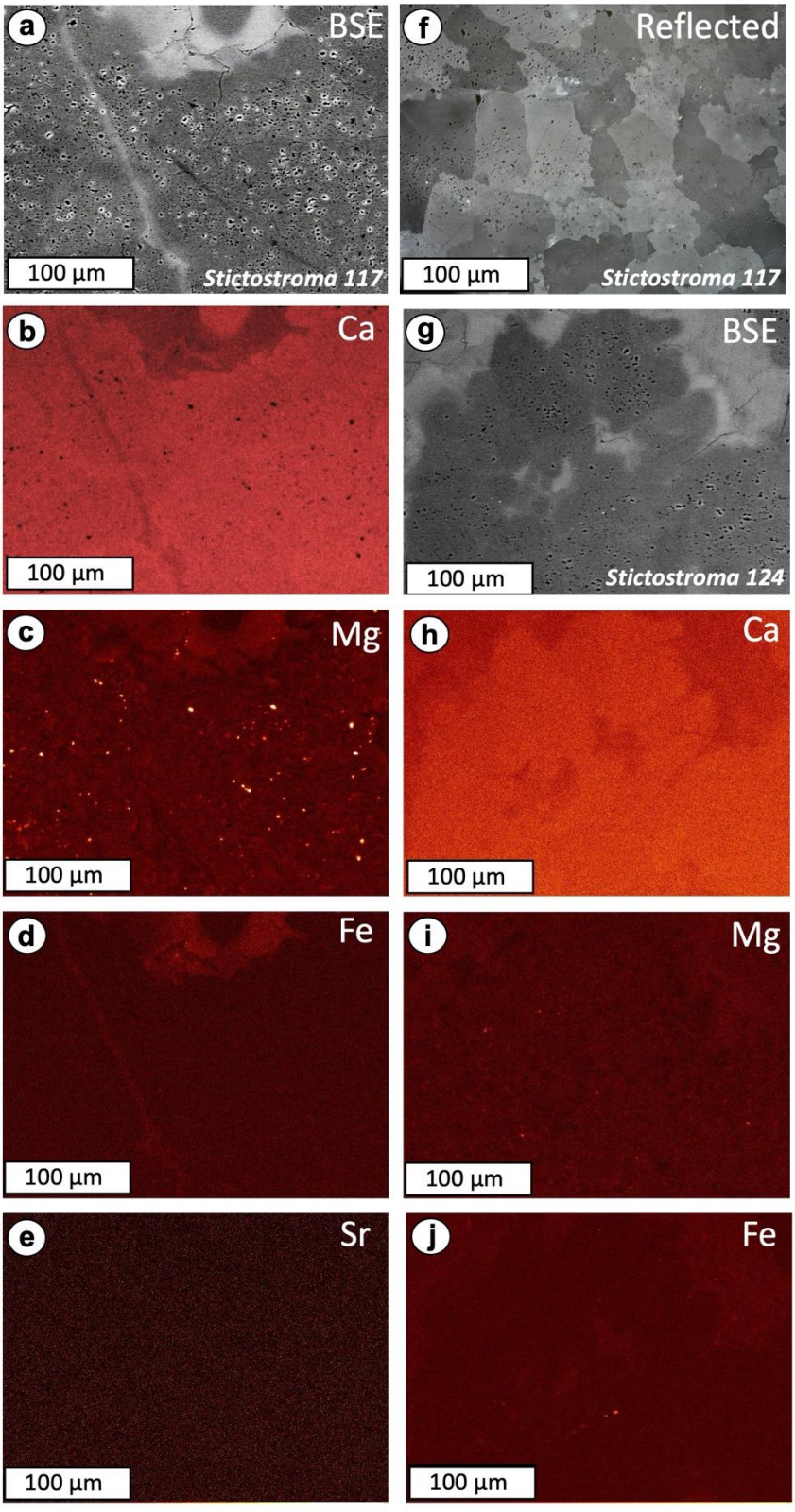

Fig. 8. *Stictostroma*, Devonian of Belgium, structure and elemental composition in two specimens of this taxon; note that this study did not examine *Stictostroma* in EBSD. **a-e** VS views of the same area. **a** shows BSE image, highlighting margin between a lamina in the lower two thirds of the photo, and gallery space in the upper one third; bright dots are inclusions in the skeletal structure. **b-e** shows elemental maps. **f** shows a reflected light image of an area near to a-e, showing the polished surface used in this study and demonstrates the recrystallised stromatoporoid structure. **g-j** VS views of the same area (g shows the margin between a lamina in the lower one third of the photo, and gallery space in the upper two thirds). h-j are elemental maps indicated on each image; in each case lighter tones represent higher concentrations of each element. As in the Silurian samples from Gotland, the images in this figure demonstrate there is very little variation of key elemental components in *Stictostroma*

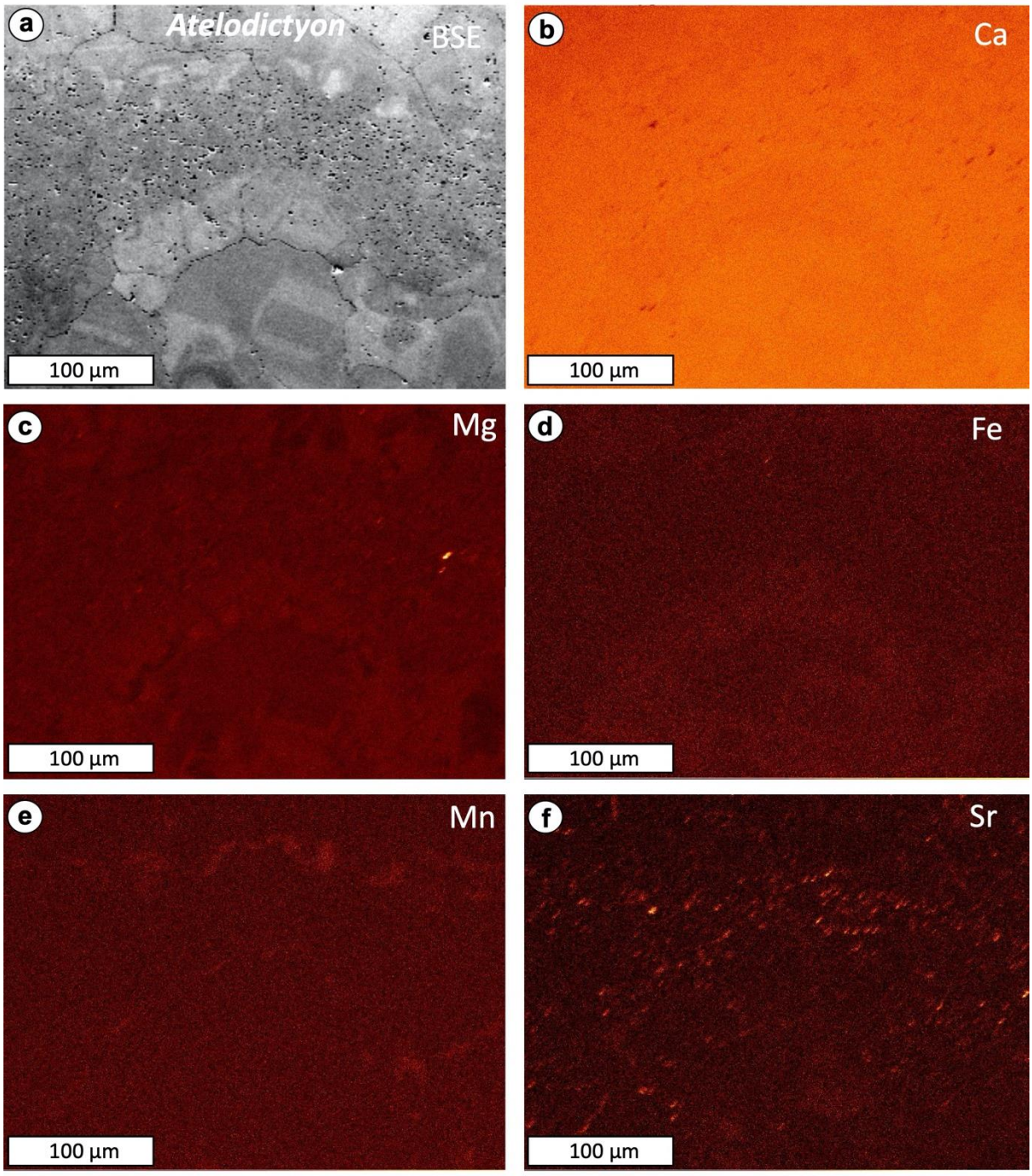

Fig. 9. *Atelodictyon*, Devonian of Belgium, structure and elemental composition in one specimen of this taxon. **a** Vertical section showing BSE image with a lamina of the stromatoporoid skeletal structure in the central one third of the picture, and gallery space in the lower and upper parts, with prominent calcite sparite. **b-f** Vertical section views of elemental maps indicated on each image, of the same area as a, showing, as in the Silurian samples (Figs. 4 and 6) and the other Devonian sample

(Fig. 8), that there is little difference between key elements of the skeleton and gallery cements

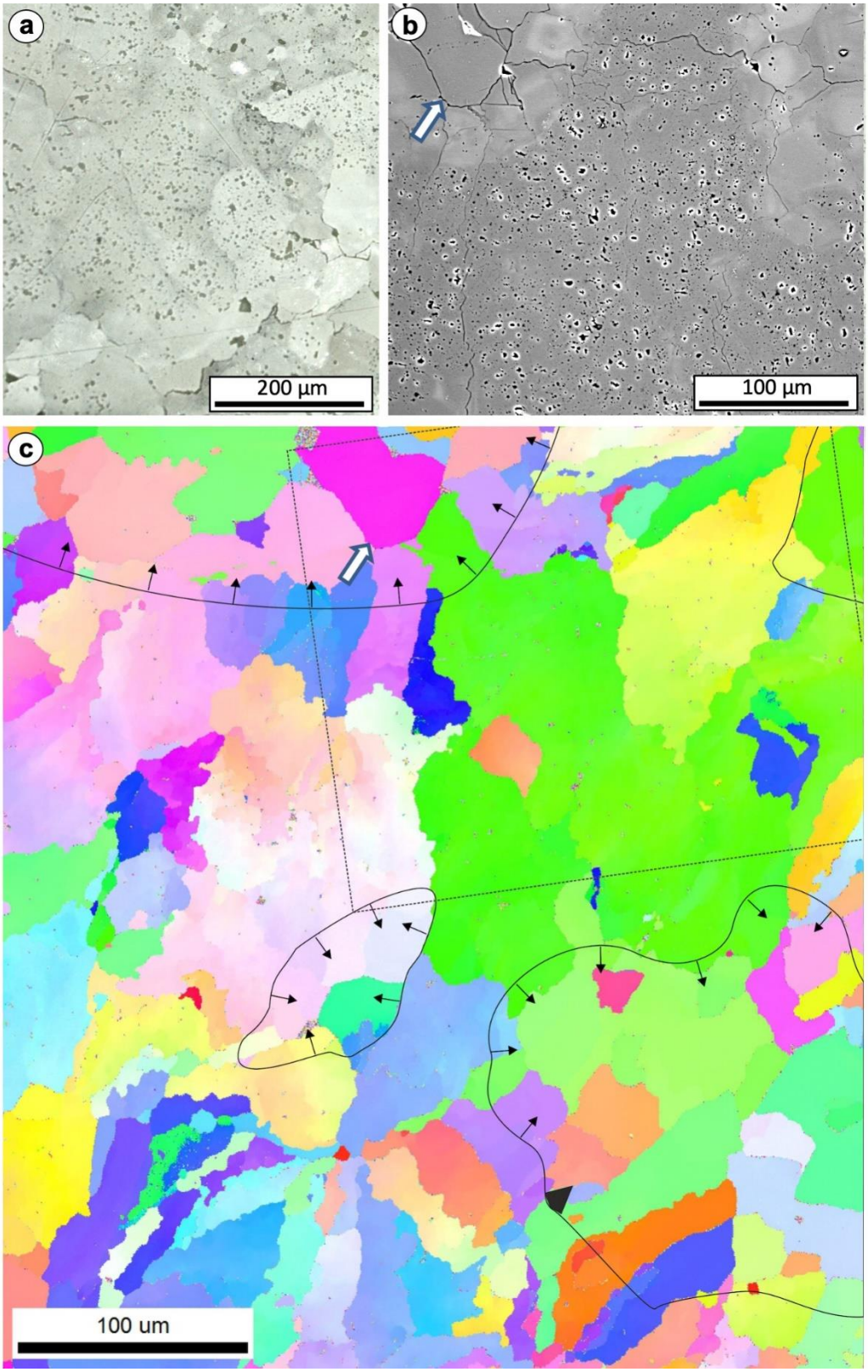

Fig. 10. *Atelodictyon*, Devonian of Belgium, skeletal structure. **a** Reflected light image from the polished surface of sample used in this study. This image is from a different area from that illustrated in b and c. **b** Vertical section of BSE of part of the

947 area in c, located by the oblique rectangle in c. This image more clearly shows the
948 speckled appearance of the stromatoporoid skeleton contrasting the clear areas of
949 gallery cement. **c** EBSD colour image of same area as a, showing a general vertical
950 orientation of crystal structure that is typical of stromatoporoids. For the colour key,
951 see Fig. 3e. Curved lines with arrows highlight the skeleton margin with arrows
952 pointing into the gallery areas. Note the subtle colour shade changes within crystals
953 illustrating shifts of crystal axes within the areas of larger crystals, evidence of
954 altered crystal bundles, discussed in the text. White arrow marks matched points in b
955 and c
956

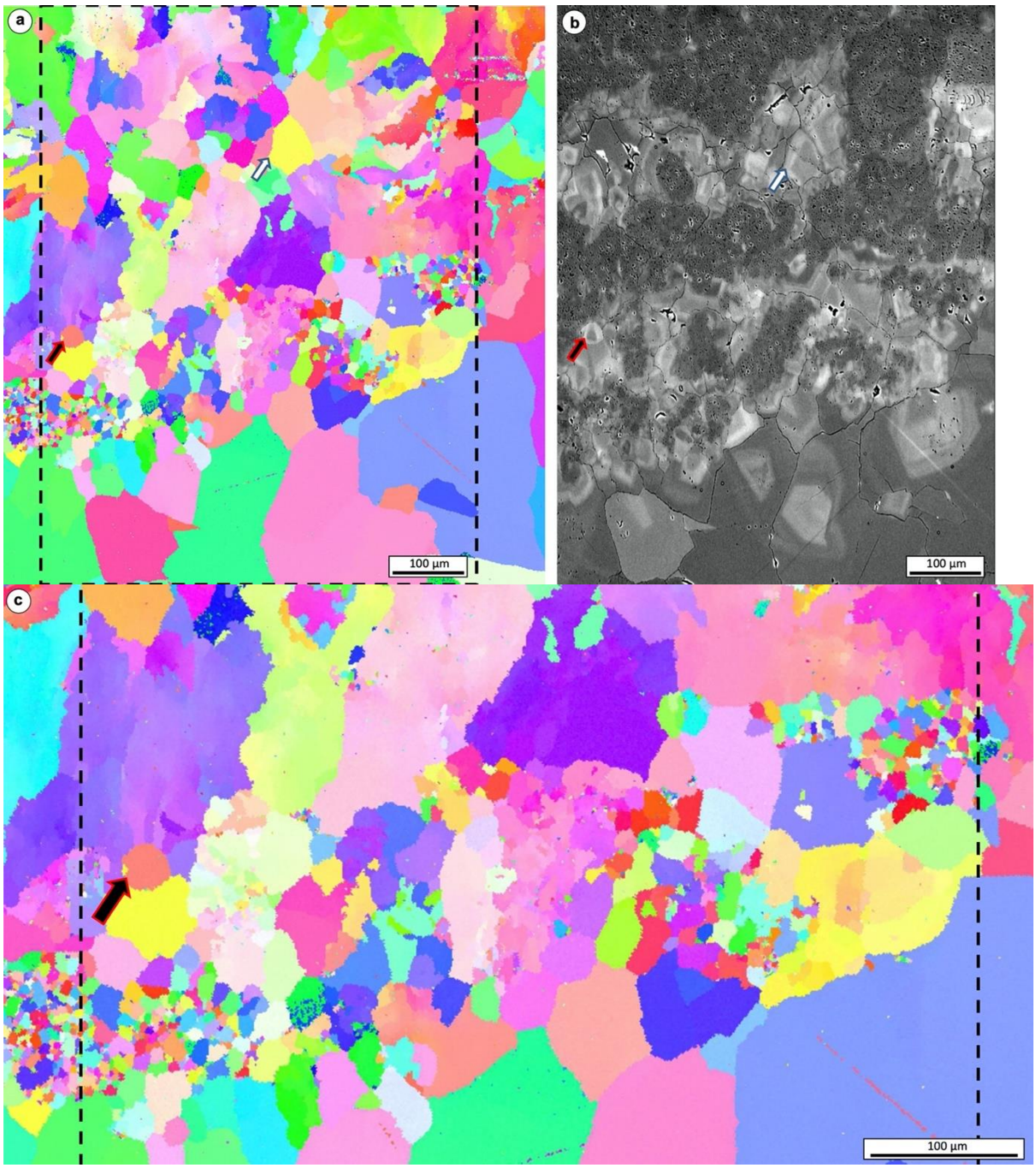

957
958
959 Fig. 11. *Atelodictyon*, Devonian of Belgium, skeletal structure. **a** Vertical section
960 showing EBSD crystallographic orientation map, where the areas of smaller crystals
961 are stromatoporoid skeleton contrasting the larger areas of gallery cement. For the

colour key, see Fig. 3e. As in the other images of stromatoporoids illustrated in this study, a general vertical orientation of crystal structure is visible here. Note the subtle colour shade changes within crystals illustrating shifts of crystal axes within the areas of larger crystals, evidence of altered crystal bundles, discussed in the text. **b** Vertical section of BSE map of the area of the box in a, white and black/red arrows mark matched points in the two images. This picture very clearly shows the speckled appearance of the stromatoporoid skeleton contrasting the clear areas of gallery cement. **c** Enlargement of a showing the subtle shading within larger crystals in more detail, illustrating small variations in sub-crystal orientation (e.g. the two large blue-purple areas upper centre and upper left)

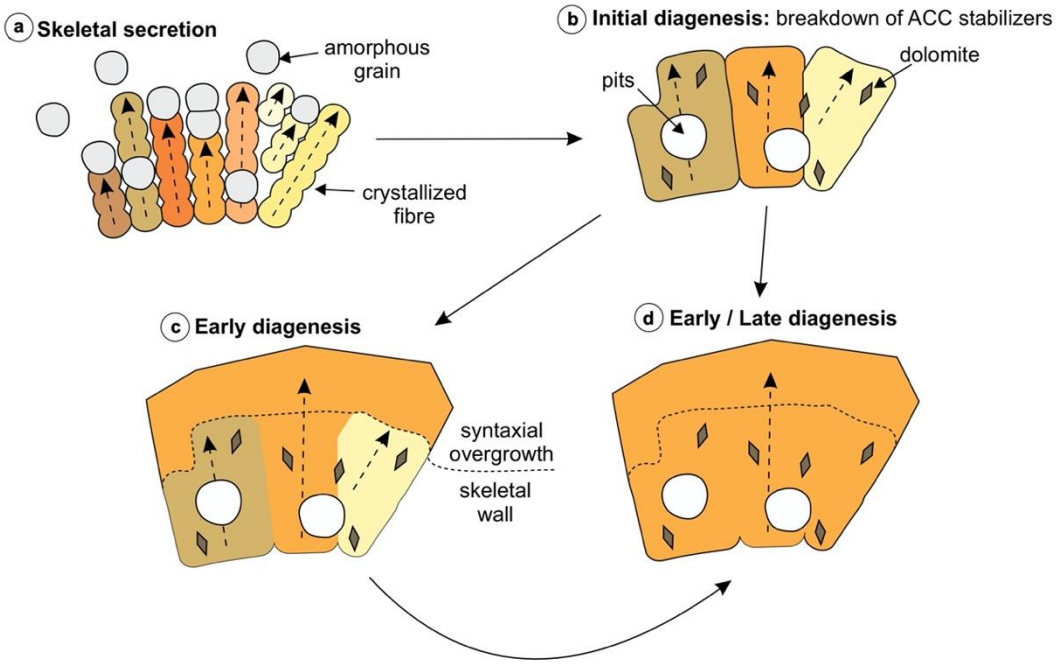

Fig. 12. Proposed diagenetic model of Palaeozoic stromatoporoid skeletons. **a** Model of skeletal secretion (based on Gilis et al. 2011) in which amorphous grains assemble to form fibres or aggregates. The initially 'mushy' amorphous grains crystallise along a propagating crystallisation front. Different colours and dashed arrows indicate different crystallographic orientations of individual crystal fibres. We propose that some amorphous grains fail to crystallise and form amorphous inclusions. **b** During initial diagenesis the amorphous inclusions disintegrate and induce localised dissolution resulting in release of Mg^{2+}, Ca^{2+}, and CO_3^{2-} ions that will re-precipitate as calcite and dolomite in the vicinity. This process leads to the coarsening of crystal fibres. **c** At the outer margins of the skeletal walls, syntaxial overgrowth results in further enlargement of calcite crystals that now extend beyond the skeleton into the galleries. Crystallographically similar adjacent domains will retain their crystallographic orientation. **d** Blocky calcite crystals with micropores, dolomite inclusions, and a syntaxial overgrowth. This could form either directly from initial diagenesis as illustrated in b by higher dissolution and the associated growth of one crystal at the expense of others, or by the transformation of a crystal with

diagenetically less stable domains of different crystallographic orientation (as shown in c) into a crystallographically homogenous single crystal

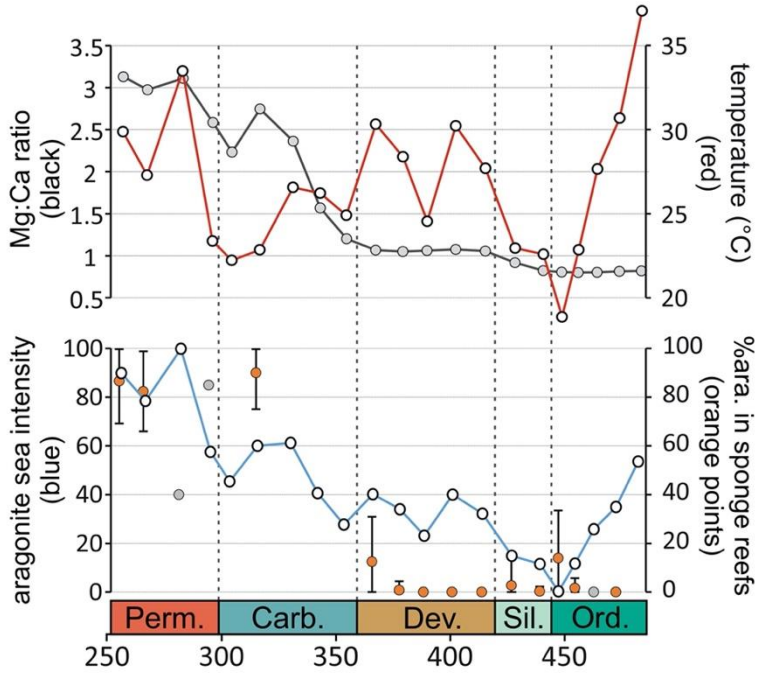

Figure 13. Aragonite-Calcite sea conditions and mineral composition of sponge-dominated Palaeozoic reefs. Upper chart shows Mg:Ca ratio (Demicco et al. 2005) and temperature estimate (Veizer & Prokhov 2015) for 21 Palaeozoic time bins. Lower chart shows combined effect of Mg:Ca ratio and temperature on non-biogenic $CaCO_3$ polymorph precipitation (based on Eichenseer et al. 2019); Orange and grey dots: average mineral composition of 341 sponge-dominated Palaeozoic reefs as found in the PARED. Orange dots = 5 or more reefs in bin, grey dots = 1-2 reefs in bin; error bars = 1 standard deviation.